Magnetic Pulse Modulators

By K. J. BUSCH, A. D. HASLEY and CARL NEITZERT

(Manuscript received March 11, 1955)

The impetus for the development of magnetic pulse modulators for radar gear stems from the extreme reliability possible for magnetic devices. Descriptions of magnetic modulators developed for this purpose are given. Mathematical treatments of both the ac and dc charged series type magnetic modulators add to the understanding of core resetting in the ac case and reveal new areas of operation in the dc case, such as a possibility of voltage amplification and automatic core resetting. Means are described for obtaining very short pulses and for absorbing unwanted stored energy in parasitics following the output pulse. These means may also be applied to other pulse modulators. Also, a way is suggested for operating the cathode of the thyratron at ground potential in a dc charged magnetic pulse modulator.

INTRODUCTION

Increasing emphasis on the reliability of the components used in electronic equipment is leading component and system designers to greater use of magnetic devices to take advantage of their almost unlimited life. These devices have been used to replace limited life items, such as hydrogen thyratrons, electron tubes, etc., or to relegate such items to a part of the circuit where long life can be obtained by operation well below rating. Examples of the application of magnetic devices to improve the reliability of radar system modulators are the ac and dc magnetic pulse modulators to be described herein.

These radar modulators provide short-duration high-voltage high-current negative pulses to a magnetron which generates microwaves for the system. An essential function of the modulator, accordingly, is one of intermittently switching a high-voltage high-current source across a load. In a typical system, the duration of the switching action might be one microsecond or less, and a thousand such switches a second would be required. A typical voltage might be 30,000 volts and the peak current

quency or a sub-multiple of it. If the supply is dc and S_1 is omitted, the repetition rate is equal to twice the frequency at which the charging inductor, L, and the capacitance of the pulse network resonate. If the switch is present, repetition rates which are less than this may be used. During the charging period of the network, S_2 is open and the network acts simply as a capacitor, C. When the network is fully charged and the charging current has fallen to zero, S_2 is closed. The network discharges through the pulse transformer into the magnetron load. Switch, S_2, is then opened and the cycle is repeated.

The switch, S_2, must carry a large peak current during the discharge of the network. This switch may be a spark-gap, a thyratron or a thyractor. In order that a thyractor may be used, its core must be unsaturated during the charging of the network and must saturate at the instant the network is due to discharge. Also, after the thyractor functions as a switch, its core must be reset to be ready for the next pulse.

This circuit, with a thyractor, would be a practical one except for the fact that the network must discharge through the saturated reactance of the thyractor. Since this reactance becomes part of the network during discharge, it limits the shortness of the pulse obtainable. As a practical matter, this reactance cannot be made arbitrarily small since the cross-sectional area of the core, the flux density and the number of turns of wire on the winding must satisfy the relation

$$NAB = \int e\,dt \tag{3}$$

during the charging period without prematurely saturating the core.

To avoid this difficulty, a step-by-step method of charging the network is used. The saturation flux linkages of the thyractors may be made smaller with each step providing a large enough ratio of saturated to un-

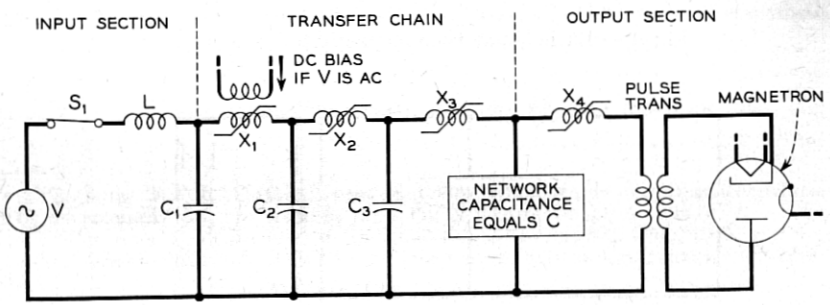

Fig. 3 — Basic series type magnetic pulse modulator.

saturated inductance is provided in the thyractor. Fortunately, the permalloys are ideal for this use and three or four thyractors are all that are needed to cut the charging time of the network from the order of thousands of microseconds to the order of a microsecond. Referring to Fig. 3, the inductor, L, has the same function as it had in Fig. 2, and, neglecting losses, the capacitors, C_1, C_2 and C_3 each may have a value equal to the capacitance of the network. The thyractors X_1, X_2, X_3 and X_4 have descending values of saturation flux linkages. With this circuit, when the first capacitor is charged to its peak voltage, X_1 saturates and connects C_2 across C_1 through the saturated inductance of X_1. It will be shown later that all the energy stored on C_1 will be transferred to C_2 in a time equal to one-half cycle of the resonant frequency of the saturated inductance of X_1 and the capacitance of C_1 and C_2 in series. Once C_2 is charged, X_2 saturates and the charge on C_2 is transferred to C_3 in a shorter time than the previous transfer since the saturated inductance of X_2 is less than that of X_1. This process continues until the network is charged. The time of charge of the network is so fast that thyractor, X_4, needs only a few turns and its saturated inductance usually ends up being about that of a section of the network.

It is seen from the above that the thyractors are designed to have descending values of saturated inductance as the energy is stepped from one capacitor to the next, until a value is reached in the last thyractor, X_4, that is small enough to be incorporated into the pulse network. Under this circumstance, the switching action of the last thyractor may be considered as ideal. Referring again to Fig. 3, it is the section of the circuit labeled "Transfer Chain" that provides this desired decrease in charging time of the network or, in other words, pulse shortening action. This action and the way the thyractor cores are reset after each pulse will be given detailed attention in the Parts that follow.

Part II — AC-Charged, Series-Type, Magnetic Pulse Modulator

The circuit diagram of a typical ac charged modulator is shown in Fig. 4. Power transformer, $TR1$, transforms the voltage available from the source to the value best suited to the transfer chain. The linear reactor L_i may be on either the primary or the secondary side of the power transformer but placing it on the primary side generally results in a more economical design. The dc bias shown on the first thyractor is necessary if pulses of one polarity are to be obtained. Bias current would ordinarily be obtained from the ac source by means of a dry-disk rectifier. The linear inductance in the bias circuit decouples the bias supply from the first

thyractor and will be assumed large enough to keep the bias current constant.

For purposes of analysis, the modulator will be divided into an input section, a transfer chain and an output section. The input section, up to and including the first thyractor, will be analyzed first. It will be shown how this portion of the circuit produces one negative current pulse through thyractor X_1 for each cycle of the ac source. The action of a section of the transfer chain in converting this current pulse into a shorter current pulse will then be explained. A more detailed explanation of the transfer chain is included in Part III. With this as background, the special requirements imposed on the thyractor core material will be discussed. The output section will then be analyzed in detail and a method given for producing shorter pulses than are possible with the circuit of Fig. 4. Finally, the core resetting action, which automatically takes place between main pulses, will be analyzed.

In the actual design of a modulator, the effect of dissipation must be considered. This may be done by an approximate method, as given in Part III, or exact numerical computations may be made. However, in order to make the main action of the modulator more apparent, dissipation will be neglected in this Part.

Thyractors will be assumed to have zero reluctance cores when unsaturated. The core will be assumed to saturate suddenly when the core flux reaches its saturation value Φ_s, after which the thyractor will have a constant saturated inductance L. In order to satisfy these assumptions, the idealized hysteresis loop must have the form shown in Fig. 5.

INPUT SECTION

If the power source and the charging inductance are referred to the secondary of the power transformer, the circuit of the first section will

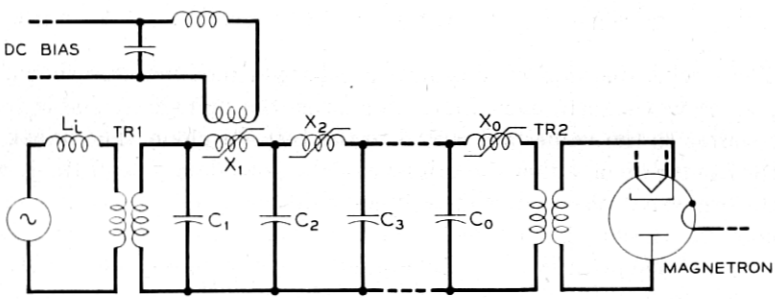

Fig. 4 — Circuit diagram of a typical ac charged series-type modulator.

be that shown in Fig. 6. The apparent source, v_i, will be assumed to have no internal impedance and to provide a sinusoidal voltage

$$v_i = V_i \sin \omega t_i \tag{4}$$

where $\omega/2\pi$ is the pulse repetition rate required at the magnetron. A set of initial conditions will be assumed for time $t_i = 0$ and will be justified by showing that the circuit returns to these conditions at the end of one cycle. These conditions are $i_i(0) = i_1(0) = I_b$, $v_1(0) = v_2(0) = 0$ and $\varphi_1(0) = -\Phi_{1s}$. In these relations, i_i, i_1, v_1 and v_2 are the instantaneous currents and voltages labeled on the circuit of Fig. 6, I_b is a constant component of i_i and i_1 which is to be evaluated, φ_1 is the core flux of thyractor X_1 and Φ_{1s} is the saturation value of φ_1. It is further assumed that all other capacitors in the chain are initially discharged and that all other thyractors are saturated in the direction of positive flux. These latter assumptions are approximate as will be seen when the resetting action is considered.

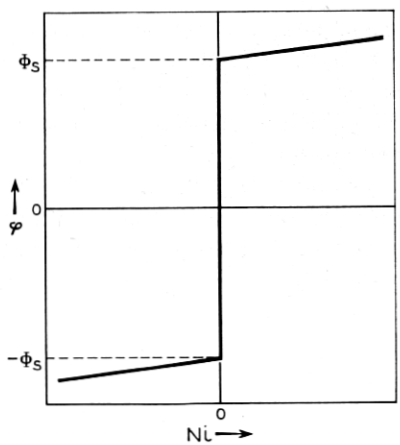

Fig. 5 — Idealized hysteresis loop upon which the theoretical analysis is based.

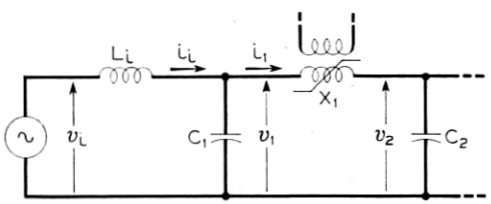

Fig. 6 — Input section of an ac charged modulator. This circuit produces one negative current pulse through X_1 for each cycle of the ac source.

The differential equations for the circuit are

$$V_i \sin \omega t_i = L_i \frac{di_i}{dt_i} + v_1 \tag{5}$$

and

$$i_1 = i_i - C_1 \frac{dv_1}{dt_i} \tag{6}$$

With the initial conditions assumed, and with L_i chosen to make $\omega^2 L_i C_1 = 1$, the solutions to these equations are

$$i_i = I_b + \frac{V_i}{2\omega L_i} \omega t_i \sin \omega t_i \tag{7}$$

and

$$v_1 = \frac{V_i}{2} (\sin \omega t_i - \omega t_i \cos \omega t_i) \tag{8}$$

In solving for these equations, it is assumed that i_1 remains constant at I_b. This is justified by the fact that v_1 becomes positive immediately after time $t_i = 0$ causing the flux φ_1 of the first thyractor to rise into the unsaturated region. The high unsaturated inducatance of the thyractor then keeps the current constant.

In the unsaturated condition the net mmf acting on the thyractor core must be zero, therefore the mmf of the main thyractor winding, due to the current I_b, must be balanced by the mmf of the bias winding. Since the bias current can be arbitrarily adjusted, the value selected should give optimum conditions in the remainder of the circuit. The proper value of I_b is

$$I_b = \frac{V_i}{2\omega L_i} \tag{9}$$

This value of I_b makes the average value of i_i equal to zero and thus avoids dc saturation in the core of the power transformer. It has the additional advantage of making the rms source current a minimum. This gives maximum source power factor and minimum copper loss in the charging choke and the power transformer. The value of the source power factor corresponding to this value of I_b is slightly over 0.96 and the rms value of i_i is 1.15 $V_i/\omega L_i$.

During the time that (7) and (8) apply, the current I_b flows through all the thyractors and the primary winding of the pulse transformer. Since none of these, except the first thyractor, have any core bias, their

cores are all held at positive saturation which is their reset condition. If the windings are dissipationless, all capacitors, except C_1, are short circuited.

With no voltage across C_2, the voltage v_1 is applied across the first thyractor. This causes its core flux φ_1 to vary in accordance with the equation

$$\begin{aligned}\varphi_1 &= \frac{1}{N_1}\int v_1\, dt_i \\ &= \frac{V_i}{2\omega N_1}(2 - 2\cos\omega t_i - \omega t_i \sin\omega t_i) - \Phi_{1s}\end{aligned} \tag{10}$$

in which N_1 is the number of turns on the main winding of X_1.

Equations (7), (8) and (10) are plotted in Fig. 7 for two cycles of the source. The source voltage v_i is included for reference. The charging current of capacitor C_1 equals $i_i - I_b$. This current is a sinusoid whose amplitude increases in direct proportion to time. During the first half cycle, C_1 charges to a positive maximum voltage of $\pi V_i/2$. The capacitor current then reverses and C_1 discharges, becoming completely discharged when ωt_i equals 4.49 radians. During the interval $\omega t_i < 4.49$, v_1, the voltage across X_1, is positive, causing φ_1 to increase. At $\omega t_i = 4.49$, φ_1 passes through a maximum value

$$\varphi_{1\max} = \frac{3.41\ V_i}{\omega N_1} - \Phi_{1s} \tag{11}$$

To avoid saturation of the core at this time, the inequality

$$2\omega N_1\Phi_{1s} > 3.41\ V_i \tag{12}$$

must be satisfied. Fig. 7 shows $\varphi_{1\max} = \Phi_{1s}$. This calls for the least amount of core material but is not an essential condition. Ordinarily a small margin of safety should be allowed.

For values of $\omega t_i > 4.49$, C_1 charges in the negative direction. The capacitor voltage reaches a negative maximum value of $-\pi V_i$ at the end of the cycle. During this time, flux φ_1 decreases and, since the integral of v_1 over a complete cycle is zero, φ_1 returns to its initial value, $-\Phi_{1s}$, at the end of the cycle. The core of thyractor X_1 then saturates and C_1 discharges through the saturated inductance into capacitor C_2. Under ideal conditions, C_1 discharges completely in a very small fraction of one cycle of the source, during which time i_i is held constant by the charging inductor. At the end of the discharge, $i_i = i_1 = I_b$, $v_1 = 0$ and $\varphi_1 = -\Phi_{1s}$ which are the same as the assumed initial conditions. Capacitor C_1 then starts to recharge and the cycle is repeated.

If (12) were made an equality instead of an inequality, the thyractor core would saturate and C_1 would discharge at the end of each half cycle. Alternate pulses applied to the chain, would be of reverse polarity and a rectifier action would be necessary at some point. In this case no bias would be required on the first thyractor and current I_b could be zero. However, the core resetting action, to be described for the chain thyractors, would be upset and those thyractors beyond the rectifier would require some other means of resetting.

It is not possible to increase the charging period beyond one full cycle

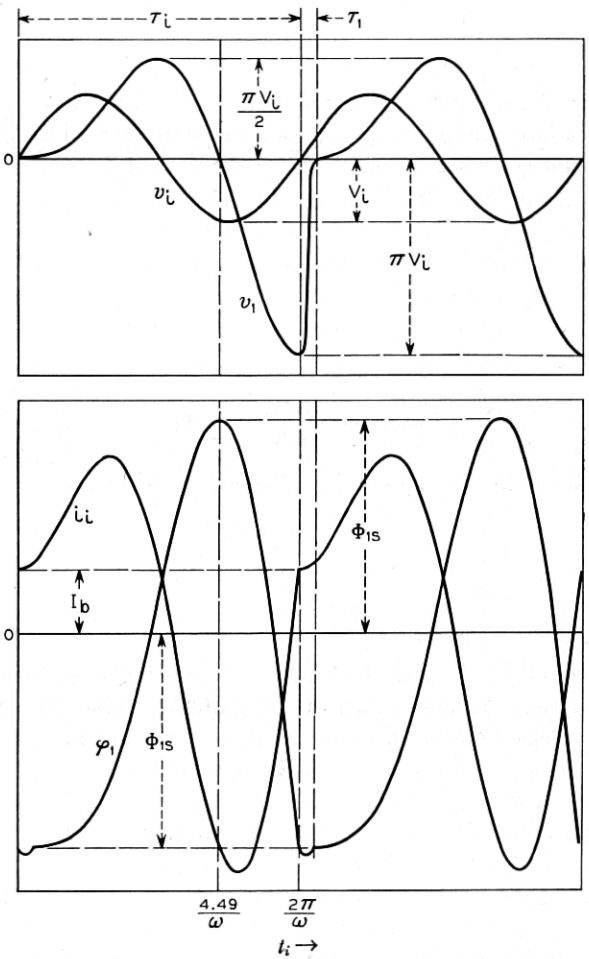

Fig. 7 — Waveforms of source voltage v_i, first-capacitor voltage v_1, source current i_i and first thyractor core flux ϕ_1 for two complete cycles of the ac source.

if the initial thyractor core flux is to be $-\Phi_{1s}$. This can be seen from (10) which gives a negative maximum value in φ_1 of $-\Phi_{1s} - 2.96\ V_i/\omega N_1$ at $\omega t_i = 7.72$ radians. This is not possible since the thyractor saturates and C_1 discharges when $\varphi_1 = -\Phi_{1s}$. The fact that φ_1 is changing at its maximum rate at $\omega t_i = 2\pi$ is advantageous though in that it makes the design of the thyractor core less critical.

Since the voltage v_1 is also across the secondary of the power transformer, the core flux of this transformer will be given by an equation similar to (10). If the average value of i_i is zero, the average value of this flux will also be zero. The transformer core must therefore be designed for a peak core flux of

$$\varphi_{T1\max} = \frac{3.41 V_i}{\omega N_s} \tag{13}$$

in which N_s is the number of secondary turns. The root-mean-square value of i_i, which is also the transformer secondary current, is 1.15 $V_i/\omega L_i$.

The linear charging reactor must be designed for a maximum energy storage of

$$\tfrac{1}{2} L_i i_{i\max}^2 = 1.82\ V_i^2 C_1 \text{ joules} \tag{14}$$

TRANSFER CHAIN

The need for and the basic action of the transfer chain have been discussed in Part I. A general analysis of a single section of the chain and of the chain as a unit is given in Part III. It will suffice here to set down the special conditions which apply in the case of ac charging.

Figure 8 shows the 1st and 2nd sections of the chain. As previously stated thyractor X_1 saturates once each cycle allowing C_1 to discharge into C_2. This occurs when v_1 has its maximum negative value. In the case of the ac charged modulator, it is desirable that C_1 be completely discharged when X_1 becomes unsaturated. In the absence of dissipation,

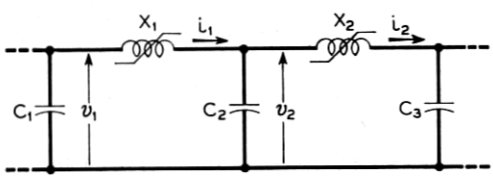

Fig. 8 — Circuit diagram of the first two sections of the transfer chain. The chain serves to produce successively shorter current pulses through each thyractor.

this requires that $C_1 = C_2$. In this case, all of the energy stored in C_1 will be transferred to C_2 and the peak value of v_1 will be the same as the peak value of v_2, that is $-\pi V_i$.

During the discharge of C_1 into C_2, with a negligibly small error,

$$i_1 = I_b - \frac{\pi V_i}{\omega_1 L_1} \sin \omega_1 t_1 \tag{15}$$

$$v_1 = -\frac{\pi V_i}{2} (1 + \cos \omega_1 t_1) \tag{16}$$

$$v_2 = -\frac{\pi V_i}{2} (1 - \cos \omega_1 t_1) \tag{17}$$

and since v_2 also appears across thyractor X_2

$$\varphi_2 = \frac{-\pi V_i}{2\omega_1 N_2} (\omega_1 t_1 - \sin \omega_1 t_1) + \Phi_{2s} \tag{18}$$

In these equations i_1, v_1 and v_2 are the current and voltages designated in Fig. 8, φ_2 is the core flux of X_2, N_2 is the number of turns on X_2, L_1 is the saturated inductance of X_1, t_1 is the time measured from the instant X_1 saturates and ω_1 is resonant angular frequency of the discharge circuit.

Figure 9 shows curves of v_1, v_2, i_1 and φ_2 plotted versus t_1. The current pulse in i_1 is one half of a cycle of a sine wave superimposed on the constant value I_b. The duration of this pulse is $\tau_1 = \pi/\omega_1$. This circuit transfers the stored energy from C_1 to C_2. During this interval φ_2 varies from positive to negative saturation. If thyractor X_1 is designed to satisfy the equation

$$4N_2\Phi_{2s} = \pi V_i \tau_1 \tag{19}$$

φ_2 will reach negative saturation at the same time that $v_1 = 0$ and $v_2 = -\pi V_i$. Since at this time $i_1 = I_b$, X_1 will become unsaturated after which i_1 will be held at I_b. When X_2 saturates, C_2 starts to discharge into the third capacitor. The current pulse through X_2 is shown as i_2 in Fig. 9. The duration of this pulse is

$$\tau_2 = \frac{\pi}{\omega_2} = \pi \sqrt{\frac{L_2 C_2 C_3}{C_2 + C_3}} \tag{20}$$

in which $C_3 = C_2$ for optimum operation of the dissipationless ac charged modulator.

The current pulse thus travels down the chain, becoming greater in magnitude and smaller in duration in each successive section. The ratio

of τ_1 to τ_2 can be shown to be approximately proportional to the saturation flux density and the square root of the core volume of thyractor X_2. It is also inversely proportional to the square root of the pulse energy. Theoretically this ratio can be made large at pleasure but it is generally more economical to use several sections to obtain the desired reduction in pulse duration.

When dissipation is considered the capacitors should be graded in size and the peak capacitor voltage should increase toward the input of the chain. A simple approximate method of including dissipation consists of raising the peak voltage of say capacitor C_1 so that it will have an excess of stored energy equal to the estimated copper loss in X_1 and core loss in X_2. An alternate approximate method is given in Part III.

Neither of the above methods give a satisfactory account of the core loss in that portion of the chain where the pulse becomes very short. Unless the product of C_2 and the shunt coreloss-resistance of X_2 is large, the analysis of Fig. 8 should be made on an exact basis. This involves 3rd

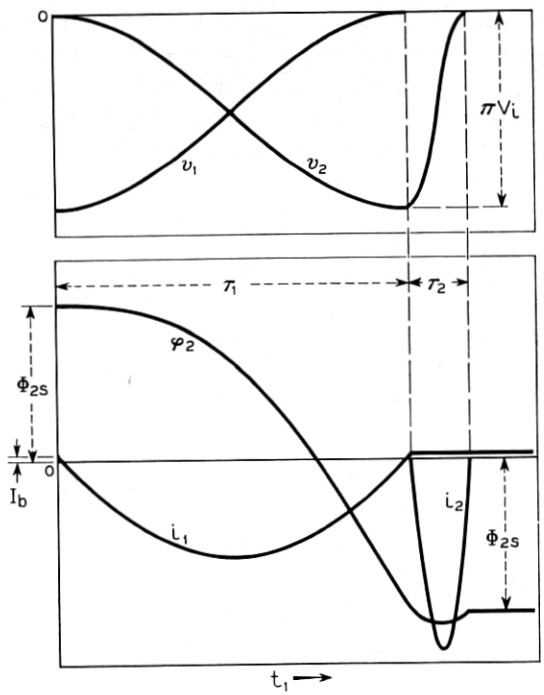

Fig. 9 — Curves illustrating the reduction in the current-pulse width from the first to the second thyractor. Capacitor voltages and thyractor core flux are also shown. These curves are typical of all of the transfer sections.

order differential equations and therefore should be done numerically for individual cases.

CORE CONSIDERATIONS

The cores of thyractors require special consideration. It has been previously assumed that the thyractor cores have zero reluctance when unsaturated and become suddenly and completely saturated at a certain value of flux. The practical approximation of this is a core that reaches complete saturation at a small value of magnetizing force. This inherently requires that the unsaturated permeability be high. Examples of core materials that meet this requirement are the nickel-iron alloys such as deltamax, molybdenum permalloy and supermalloy. Others of equal importance exist but they will not be discussed here. The chief advantage of deltamax over the other two is its high saturation flux density. Its use is therefore indicated when the saturating time is long, as in the case of the input thyractor. The fact that its hysteresis loop has a striking rectangular appearance is, in itself, no great virtue for this application.

For thyractors following the first, the swing in flux linkage is much smaller and the high saturation flux of deltamax is not required. In all thyractors, the flux swings from saturation in one direction to saturation in the other and back again for each pulse applied to the magnetron. With respect to core loss, supermalloy is superior to both deltamax and molybdenum permalloy in that it has a higher resistivity and a much lower hysteresis loss. Supermalloy is also suitable for use in the first thyractor in certain cases where the repetition rate is high.

In order to utilize the advantages of these high-permeability materials, the thyractor cores must be of the gapless wound-tape type. In most cases, the tape thickness will be made smaller as the output of the modulator is approached and may reach values below one mil.

OUTPUT SECTION

When a rectangular voltage pulse of relatively long duration is required for the magnetron, the output capacitor, C_0 of Fig. 4, is replaced by a line-type pulse-forming network having a total capacitance equal to the normal value of C_0. During the relatively long charging period, the network acts like a capacitance C_0, whereas during the relatively short discharge period it acts as a pulse-forming network. The saturated inductance of the output thyractor is in series with the network during discharge. This adds to the design complication. Either the thyractor saturated inductance must be made small enough to cause negligible

distortion in the pulse shape or the network must be designed to include the inductance as part of the network. In the former case, the reduction in pulse width by the output section of the modulator is appreciably less than could otherwise be obtained.

As the required magnetron pulse width decreases, the output thyractor, the pulse transformer and the shunt capacitance cause deterioration of the pulse shape to the extent that a pulse-forming network can hardly be justified. If a capacitor is used instead of a network, the output section can be designed as a unit in accordance with the following analysis.

Fig. 10 shows the output section with all elements referred to the secondary of the pulse transformer. In this circuit L_0 represents the sum of the transformer leakage inductance and the saturated inductance of the output thyractor, capacitance C_M is the sum of the transformer capacitance and the magnetron capacitance. Current i_M is thus the total

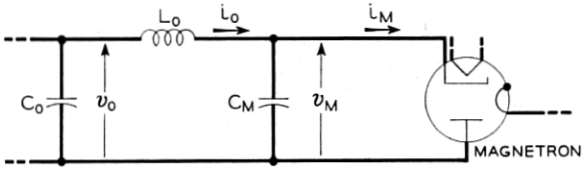

Fig. 10 — Output section with a magnetron load. All elements are referred to the secondary of the pulse transformer.

magnetron current less the current required to charge the magnetron capacitance.

For the period under consideration, v_0 has an initial value $-V_0$ and the initial values of i_0, v_M and i_M are all zero. The thyractor saturates at the beginning of the period. Capacitor C_0 discharges through L_0 into C_M until v_M reaches the magnetron firing voltage, $-V_M$. If the magnetron is approximated by a dissipationless diode in series with a biasing emf, v_M then remains constant while C_0 continues to discharge through the magnetron.

During the charging of C_M

$$i_0 = -\frac{V_0}{\omega_0 L_0} \sin \omega_0 t_0 \tag{21}$$

where

$$\omega_0^2 L_0 \frac{C_0 C_M}{C_0 + C_M} = 1 \tag{22}$$

$$v_0 = -\frac{V_0 C_0}{C_0 + C_M} - \frac{V_0 C_M}{C_0 + C_M} \cos \omega_0 t_0 \tag{23}$$

and

$$v_M = -\frac{V_0 C_0}{C_0 + C_M} (1 - \cos \omega_0 t_0) \tag{24}$$

in which t_0 is measured from the instant that X_0 saturates.

When $v_M = -V_M$ at $t_0 = \tau_0$, the magnetron fires. At this time

$$v_M(\tau_0) = -V_M = -\frac{V_0 C_0}{C_0 + C_M} (1 - \cos \omega_0 \tau_0) \tag{25}$$

from which

$$\cos \omega_0 t_0 = 1 - \frac{V_M}{V_0} \frac{C_0 + C_M}{C_0} \tag{26}$$

In addition,

$$v_0(\tau_0) = -V_0 + V_M \frac{C_M}{C_0} \tag{27}$$

and

$$i_0(\tau_0) = \frac{-V_0}{\omega_0 L_0} \left[\frac{2V_M(C_0 + C_M)}{V_0 C_0} - \frac{V_M^2 (C_0 + C_M)^2}{V_0^2 C_0^2} \right]^{1/2} \tag{28}$$

After the magnetron fires, v_M remains constant at $-V_M$ and

$$i_0 = i_M = \frac{v_0(\tau_0) + V_M}{\sqrt{L_0/C_0}} \sin \frac{t_0 - \tau_0}{\sqrt{L_0 C_0}} + i_0(\tau_0) \cos \frac{t_0 - \tau_0}{\sqrt{L_0 C_0}} \tag{29}$$

If the magnetron current pulse has a width τ_M at its base, and it is assumed that C_0 is completely discharged and that $i_0 = 0$ at the end of the magnetron current pulse, then from (29)

$$\frac{v_0(\tau_0) + V_M}{\sqrt{L_0/C_0}} \sin \frac{\tau_M}{\sqrt{L_0 C_0}} + i_0(\tau_0) \cos \frac{\tau_M}{\sqrt{L_0 C_0}} = 0 \tag{30}$$

Also, since $v_0 = 0$ the voltage across L_0 must equal V_M, or

$$L_0 \left. \frac{di_0}{dt_0} \right|_{t_0 = \tau_0 + \tau_M} = V_M$$

that is

$$[v_0(\tau_0) + V_M] \cos \frac{\tau_M}{\sqrt{L_0 C_0}} - \sqrt{\frac{L_0}{C_0}}\, i_0(\tau_0) \sin \frac{\tau_M}{\sqrt{L_0 C_0}} = V_M \tag{31}$$

Combining (30) and (31) and substituting the values of $v_0(\tau_0)$ and $i_0(\tau_0)$ from (27) and (28) respectively and simplifying gives

$$\frac{C_0V_0^2}{2} + \frac{C_MV_M^2}{2} = C_0V_0V_M \tag{32}$$

The first term on the left is the energy initially stored in C_0 and the second term is the energy remaining in C_M at the end of the magnetron current pulse. The difference between these energies is the magnetron pulse energy W_M, that is

$$\frac{C_0V_0^2}{2} - \frac{C_MV_M^2}{2} = W_M \tag{33}$$

When C_M is negligibly small these equations are identical since for this case $V_0 = 2V_M$. In the case being considered here, however, they may be solved for V_0 and C_0 giving

$$V_0 = V_M \frac{2W_M + C_MV_M^2}{W_M + C_MV_M^2} \tag{34}$$

and

$$C_0 = \frac{1}{V_M^2} \frac{(W_M + C_MV_M^2)^2}{2W_M + C_MV_M^2} \tag{35}$$

If the chain capacitance is given, (35) fixes the pulse transformer turns ratio after which (34) fixes the chain voltage. On the other hand, if the chain voltage is given, these equations determine the turns ratio and the chain capacitance.

It can also be shown that

$$\cos \frac{\tau_M}{\sqrt{L_0C_0}} = 1 - \frac{V_0}{V_M} + \frac{C_M}{C_0} \tag{36}$$

and

$$\cos \sqrt{\frac{C_0 + C_M}{L_0C_0C_M}}\,\tau_0 = 1 - \frac{V_M}{V_0}\frac{C_0 + C_M}{C_0} \tag{37}$$

from which L_0 and τ_0 are found.

Equations (34) through (37) assume that the magnetron pulse energy and pulse width are specified and that for a given magnetron, its shunt capacitance and firing voltage are known. If these quantities are not known, some other form of the equations may be more useful.

The shape of the magnetron current pulse depends upon the fraction

of the total energy left in C_M. Fig. 11 shows curves of i_0, i_M and v_M versus t_0 measured from the instant that the output thyractor saturates. During time τ_0, capacitor C_M charges to the firing voltage of magnetron. During time τ_M the magnetron conducts and $i_0 = i_M$. Two curves are shown for i_M during time τ_M. It is seen that if the energy stored in C_M is less than 30.9 per cent of the magnetron pulse energy, the magnetron current pulse is a better approximation of a rectangular pulse. In the terminal case where $C_M = 0$, i_M is a complete half cycle of a sine curve.

For magnetron pulse widths less than 0.1 microsecond it becomes very difficult to make $C_M V_M^2 < .618 W_M$ and as a result the magnetron current pulse deteriorates. In addition a large fraction of the energy is left in C_M at the end of the pulse and must be dissipated in the circuit. This reduces the overall efficiency of the modulator. A definite improvement can be obtained by separating the transformer capacitance from the magnetron capacitance by placing the output thyractor on the secondary side of the pulse transformer. Figs. 10 and 11 still apply, but now C_M is the total shunt capacitance across the magnetron and C_0 is the transformer capacitance plus any added capacitance that may be required. The values of V_0, C_0, L_0 and τ_0 are again given by (34), (35), (36) and (37) respectively. The pulse transformer can be designed so that its capacitance is equal to the required value of C_0 or capacitance can be added across the secondary to make the total equal to C_0. The leakage inductance of the transformer is considered as a part of the saturated inductance of the previous thyractor.

An alternate point of view is to consider the transformer capacitance

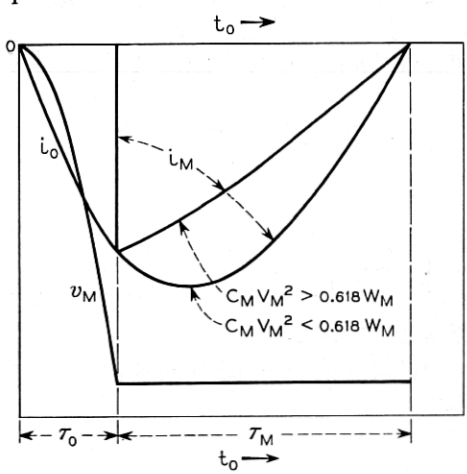

Fig. 11 — Waveforms of the magnetron current and voltage showing the effect of shunt capacitance upon the shape of the magnetron current pulse.

and leakage inductance, capacitance C_0 and the saturated inductance L_0 of the output thyractor to constitute a pulse forming network.

Placing the output thyractor on the secondary side of the pulse transformer results in a more reasonable value of L_0 unless a very high chain voltage is used. For chain voltages of the order of 10,000 volts and with very short magnetron pulses, the value of L_0 required on the primary of the pulse transformer may be a fraction of a microhenry. A much larger value is required on the secondary side so that stray inductance is far less important.

A disadvantage of placing the last thyractor on the secondary side of the pulse transformer is that the thyractor and any added capacitance across the transformer secondary must be insulated for a very high voltage, sometimes as high as 70,000 volts.

The core of the output thyractor presents special problems for very short pulses. In order to keep eddy current loss from being excessive core tape as thin as 0.25 mil may have to be used. Because of the fragility of such thin core material and the high voltage encountered, a toroidal core mounted in a core box of a high dielectric strength material such as teflon is generally desirable.

As previously mentioned, a considerable amount of energy is left in the magnetron capacitance. This energy must be dissipated in the modulator between main pulses. The result may be a considerable amount of ringing which may or may not have undesirable effects on the magnetron. In Part III the use of a damping thyractor is described which discharges C_M at the end of the magnetron pulse.

CORE RESETTING

Consideration of the first section has shown that the core flux of the first thyractor returns to its initial value at the end of each cycle. No further consideration of the resetting of this core is required. In the case of other thyractors, however, the cores must be at positive saturation at the beginning of the pulse and are left at negative saturation at the end of the pulse. Between pulses the cores must be reset to positive saturation. This resetting action is provided by the component I_b of i_i which flows even though the first thyractor is unsaturated.

The exact analysis involves long, complicated equations which add very little to a working knowledge of the modulator. To avoid including so much detail, the present analysis will be largely descriptive and only the important terms of the equations will be given.

Resetting of the second thyractor core starts at the end of the main-pulse discharge of C_2. At this time C_3 is fully charged and C_2 is dis-

charged. The voltage of C_3 is therefore applied across the second thyractor and its polarity is in the resetting direction. The resetting action of this voltage is small, if C_3 is allowed to discharge immediately, and will be neglected.

The main resetting occurs as a result of current $i_i = I_b$, which is given by (9), during the time that the first thyractor core is unsaturated. If time is measured from the instant C_2 completes its discharge of the main pulse, the voltage v_2 rises linearly according to the equation

$$v_2 = \frac{I_b t}{C_1} = \frac{\omega V_i}{2} t = \pi V_i \frac{t}{\tau_i} \tag{38}$$

Since, except for the very short time during which C_3 is discharging, $v_3 = 0$, v_2 is applied across the second thyractor and causes its core flux to rise in the positive direction in accordance with the equation

$$\varphi_2 = \frac{1}{N_2} \int v_2 \, dt = \frac{\omega V_i t^2}{4N_2} - \Phi_{2s} \tag{39}$$

Using (19), this becomes

$$\varphi_2 = \Phi_{2s} \left[\frac{2t^2}{\tau_i \tau_1} - 1 \right] \tag{40}$$

in which τ_i is the charging time and τ_1 is the discharging time of C_1.

When $t = \sqrt{\tau_i \tau_1}$, $\varphi_2 = +\Phi_{2s}$ and $v_2 = \pi V_i \sqrt{\tau_1/\tau_i}$. Assuming $\tau_i/\tau_1 = 30$ to be a typical value, this time is 0.183 τ_i and the voltage is 0.183 πV_i. When $\varphi_2 = \Phi_{2s}$, the second thyractor saturates and C_2 discharges into C_3 raising the voltage v_3 to $+\pi V_i \sqrt{\tau_1/\tau_i}$.

Fig. 12 shows curves of v_2, φ_2, v_3 and φ_3 plotted versus time measured from the end of the main discharge of C_2. Starting with the main discharge of C_1, from a to b C_1 discharges into C_2, v_2 goes negative to $-\pi V_i$ and φ_2 varies from $+\Phi_{2s}$ to $-\Phi_{2s}$. During this interval v_3 is zero and φ_3 is constant at Φ_{3s}. At point b the core of X_2 saturates. From b to c, C_2 discharges into C_3, φ_2 makes a small excursion into the saturated region, and v_2 returns to zero completing the main voltage pulse on C_2. At the same time v_3 goes negative to $-\pi V_i$ and φ_3 varies from $+\Phi_{3s}$ to $-\Phi_{3s}$. At point c the core of X_3 saturates. Immediately following c Fig. 12 shows the excursion of φ_3 into the saturated region and the return of v_3 to zero, thus completing the main voltage pulse on C_3. The effect of v_3 upon φ_2 during this discharge period τ_3 is neglected in Fig. 12. The resetting of the core of the second thyractor starts at c. The voltage and flux of the second thyractor rise according to (38) and (39) respectively. At d, the core of X_2 saturates in the positive direction. Between d and e

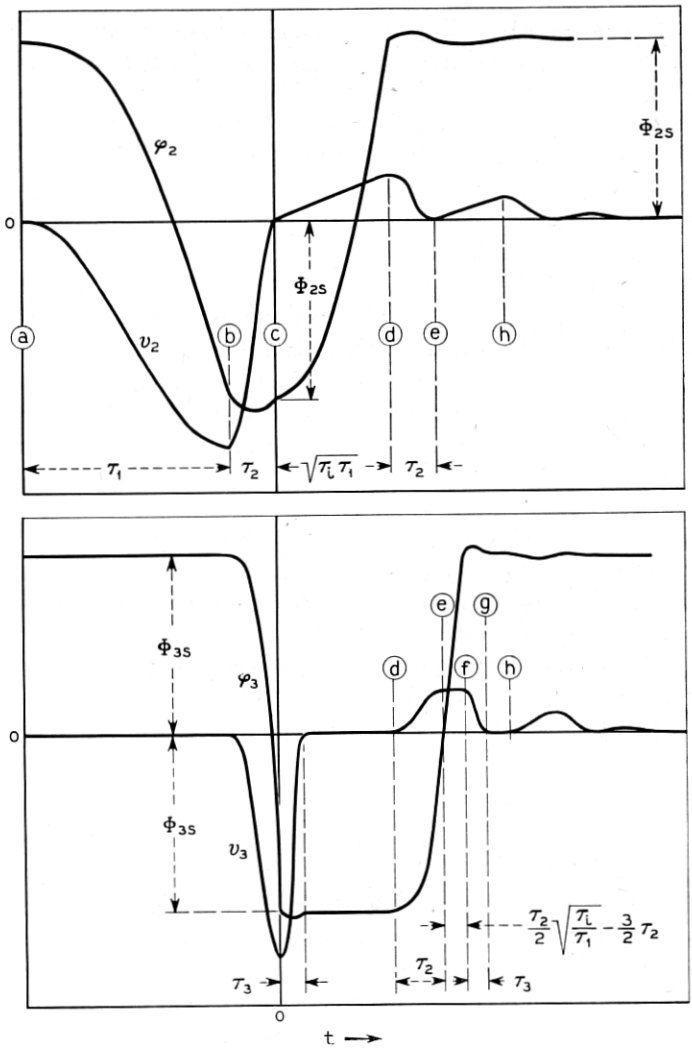

Fig. 12 — Curves of capacitor voltages and core fluxes illustrating the resetting action, of the cores of X_2 and X_3, between main pulses. This action is made possible by the core bias of X_1.

C_2 discharges into C_3. This discharge is of the same nature as the main pulse discharge in the interval b — c except that the variation is reversed and the magnitude of the voltage is much smaller. The time required, however, is the same, that is τ_2. The third thyractor does not saturate immediately at the end of this discharge because of the low

voltage. A charge is thus trapped on C_3 for an additional time equal to $\tau_2/2\sqrt{\tau_i/\tau_1} - \frac{3}{2}\tau_2$. At f the core of X_3 saturates and C_3 discharges into C_4.

A positive-going pulse is thus formed on C_2 in the interval c – d. This pulse is transferred to C_3 in the interval d – e, to C_4 in the interval f – g and so on along the chain. In the dissipationless case this pulse should reset all of the thyractor cores.

However the current I_b given by (9) continues to flow through the first thyractor. At point e, therefore, C_2 starts to recharge and v_2 again rises linearly. In the interval e – g the voltage across the second thyractor is the difference between v_2 and v_3. Since at first $v_3 > v_2$, φ_2 makes a small excursion into the unsaturated region. At g, v_3 becomes zero and φ_2 returns to positive saturation at h. A second positive-going pulse is thus formed on C_2 in the interval e – h. This pulse also moves down the chain.

This action continues, each pulse being smaller and shorter than the preceding one. Beyond h Fig. 12 is not intended to be accurate but shows in a qualitative manner that all capacitor voltages approach zero and all core fluxes approach positive saturation as required for the initial condition for the next main pulse.

In Fig. 12 the time intervals are not shown in their true relative magnitudes but are, in each case, made large enough to show the curve shape. Actual oscillograms will also show considerable deviations from Fig. 12 because of dissipation and because of small charges left on the capacitors by the main pulse.

Part III. DC-Charged Series-Type Magnetic Pulse Modulator

The dc-charged series-type magnetic pulse modulator to be discussed in this part draws power from a dc source and provides unidirectional high-voltage, short-duration pulses to a load. The basic differences between the ac- and dc-charged magnetic modulators are the type input sections required, the resulting limitations imposed upon the first section of the transfer chain, and the manner in which the saturable elements of the chain are reset.

Four input or charging circuits that periodically charge a capacitor from a dc source at a rate determined by an external trigger supply are shown in Figure 13. All these arrangements may be used for either resonant or linear charging. The first or input stage of the charging circuits shown in parts a and b of this figure are familiar arrangements employed in other type modulators. The diode indicated in Figure 13(b) permits resonant operation when the charging period is much smaller

than the pulse repetition period, or when a variable inter-pulse period is required. After C_1 in either of these two circuits has attained its desired voltage either by resonant or linear charging, the switching element is activated by an external trigger voltage and the stored energy is transferred to C_2 in a time interval short compared to the charging time of C_1. The switch is then re-opened by the completion of this transfer action and by the removal of the trigger voltage, and C_1 again begins to charge while C_2 is discharged by the action of the transfer chain (not shown in the figure).

The diode of Figure 13(b) can be replaced by the active switching device since it, too, normally has rectifying properties. This arrangement shown in Figure 13(c) operates the switching device at a lower peak current since the charging time of C_1 is long compared to that of C_2. However, it does introduce an additional large delay between the start of the trigger pulse and the generation of the modulator output pulse.

Figure 13(d) is a special charging arrangement suggested by Professor C. Neitzert that provides energy during part of the charging period of C_1 to reset the saturable elements of the transfer chain, in a manner similar to the resetting action obtained in the pulse transformer of a line type modulator. In addition, it permits operation of one element of the active switch at ground potential, which is advantageous if filamentary power is required in this device.

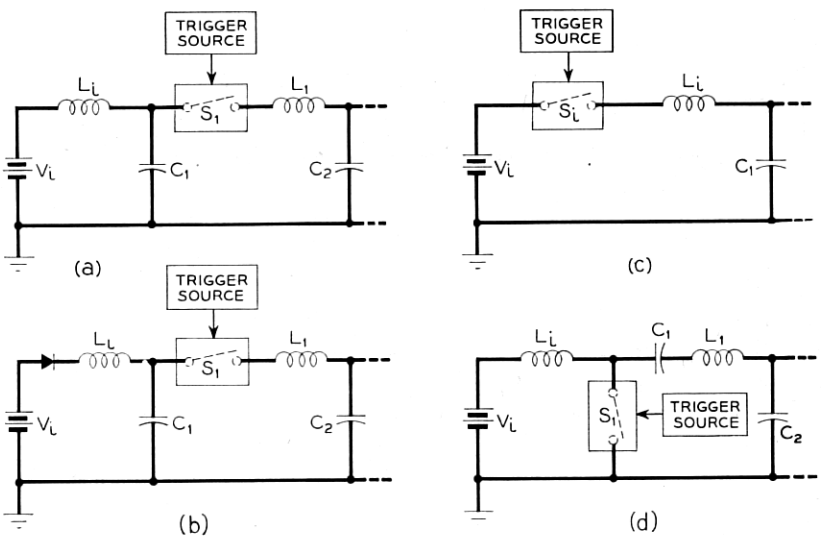

Fig. 13 — DC-charging circuits.

A typical dc-charged magnetic modulator, consisting of an input section, n transfer sections, an output section, a damping section, and load is shown in Figure 14.[5] The remainder of this part will be restricted to the analysis and discussion of the input section, a typical transfer section, and the damping section, since the response of the output section and the characteristics of a magnetron load have been treated in detail in Part II. After this is done, a composite analysis of the input section and transfer chain will be made by drawing upon the results of the first two analyses.

Before this is undertaken, certain assumptions that involve all sections and the modulator operation in general will be made. These assumptions embody an attempt to include the effect of losses which have pronounced influence on observed modulator performance. In order to facilitate the mathematical treatment of the problem, only series dissipative elements will be used. Generally, a good approximation is obtained by the following assumptions:

1. The dc source will be considered ideal.
2. The constant voltage drop generally associated with the active switching device during the charging period will be subtracted from the ideal source potential yielding a net source potential of V_i.
3. No current will flow through either an open active switching device or an unsaturated thyractor.
4. The core losses associated with any thyractor and transformer

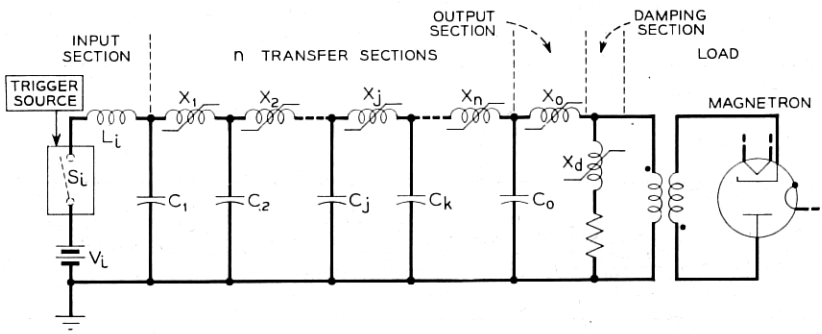

Fig. 14 — Typical dc-charged magnetic modulator.

[5] In this figure, the typical modulator operates from a dc source of positive potential and employs the active switch in the first section. This potential is used, rather than a negative one which would appear more practical, in order to facilitate the analysis that follows. The active switch could have been employed in the second section but since the only difference between such an arrangement and the one indicated is merely a matter of triggering no generality has been sacrificed.

will be represented by a series resistance in the preceding section, effective only during the time the switch associated with this section is closed.

5. The winding losses associated with any thyractor and transformer will be represented by a series resistance in the section associated with the element, effective only during the time the switch of this section is closed.

6. All capacitors will be considered lossless.

An equivalent circuit of the typical modulator based on the above assumptions is shown in Figure 15. In this figure the inductances L_1, L_2, L_j, L_n, L_0 and L_d represent the saturated inductances of the thyractors. Inductance L_t and capacitance C_d are the leakage inductance of the transformer and the distributed capacitance of the transformer and magnetron, respectively. The losses associated with the practical transformer have been included in resistances R_n and R_0 as explained in the assumptions.

Assume that a pulse of energy has been initiated down the chain and this energy is now stored in a capacitor between C_2 and C_j, while the preceding pulse has been completely dissipated in the damping section and load. Hence, the sections shown explicitly in Figure 15 are in an inactive or quiescent state. However, voltages may still exist on the capacitors of these sections, and these quiescent voltages are indicated in the figure. The energy storage associated with these voltages makes possible, as will be demonstrated later, a second method of stably operating the saturable elements without the necessity of bias windings. Now,

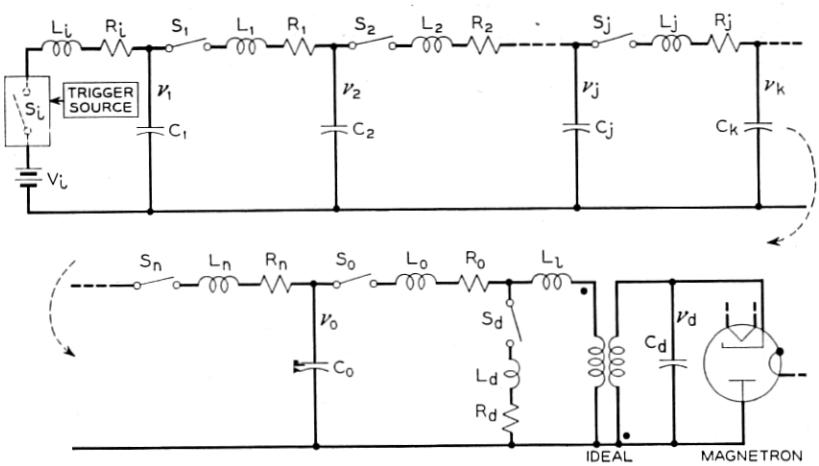

Fig. 15 — Equivalent circuit of typical dc-charged magnetic modulator.

if the assumption is made that all thyractor switch closures are initiated only when the capacitor preceding the switch stores all the available pulsed energy and the switch is re-opened when this energy, less losses, is transferred to the following capacitor, the circuit operation will be completely defined. Such an assumption means that for each pulse of energy initiated down the chain by the switch S_i, the switches close and subsequently re-open only once; that is, secondary saturations of any element are precluded.[6]

INPUT CHARGING SECTION

The input charging section of Figure 15 is shown in detail in Figure 16. Observe that the rectifying property usually associated with the active switching device is indicated explicitly by the presence of an ideal diode

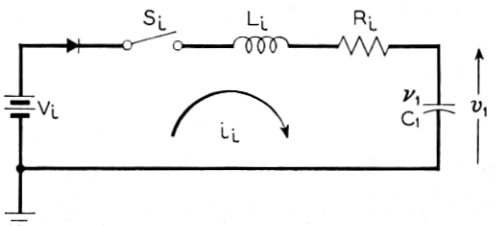

Fig. 16 — Equivalent circuit of input charging section.

in this figure. Although this circuit has already been thoroughly analyzed in past work on charging circuits,[7] the resonant charging case will be briefly treated here in order to provide the necessary background material to support the later discussion on the over-all modulator performance.

At the time switch S_i closes, time t_i equals zero, the current through the charging inductor L_i is zero, and the capacitor C_1 is charged to v_1. For these quiescent conditions, the current i_i through the switch is of the form

$$i_i = \frac{V_i - v_1}{L_i \omega_i} \epsilon^{-\alpha_i t_i} \sin \omega_i t_i \tag{41}$$

[6] Possibly it would be more desirable to store energy in either or both of the first and last capacitors of the chain that generate, during the period that the modulator is inactive, secondary voltage pulses of the proper polarity traveling in a direction which would tend to reset all magnetic elements. Such operation, however, will not be considered here.

[7] G. W. Glasoe and J. V. Lebacqz, Pulse Generators, McGraw-Hill Book Company, Inc., 1948.

where

$$V_i > \nu_1 \tag{42}$$

$$\alpha_i = \frac{R_i}{2L_i} \tag{43}$$

$$\omega_i = \sqrt{\beta_i^2 - \alpha_i^2} \tag{44}$$

and

$$\beta_i = \sqrt{\frac{1}{L_i C_1}} \tag{45}$$

for the oscillatory case. This is the only case of interest, since under this condition the charging current eventually tends to reverse, consequently initiating deactivation of the switch. This deactivation is completed by removal of the trigger voltage if it is still present. It is seen from equation (41) that the current is unidirectional over the period τ_i, the charging time of the section, where τ_i is

$$\tau_i = \frac{\pi}{\omega_i} \tag{46}$$

The voltage across C_1 as a function of time t_i is v_1, where

$$v_1 = V_i - [V_i - \nu_1]\left[\frac{\alpha_i}{\omega_i}\sin \omega_i t_i + \cos \omega_i t_i\right] \epsilon^{-\alpha_i t_i} \tag{47}$$

Since, as previously noted the charging current through C_1 has been unidirectional during the entire charging period, capacitor C_1 will be charged to its maximum voltage V_1 at the end of this period, that is, at time t_i equals τ_i. From (47) this peak voltage is

$$V_1 = V_i + (V_i - \nu_1)\delta_i \tag{48}$$

where δ_i, the loss factor of the input stage, is

$$\delta_i = \epsilon^{-\alpha_i \tau_i} \tag{49}$$

Equation (48) may also be written in the following form:

$$V_i = \left[\frac{1}{1 + \delta_i}\right] V_1 + \left[\frac{\delta_i}{1 + \delta_i}\right] \nu_1 \tag{50}$$

Upon normalizing the voltages of equations (48) and (50) and rearranging the following simple linear functions result:

$$\underline{V_1} = (1 - \underline{\nu_1})\delta_i + 1 \tag{51}$$

$$\underline{V_1} = (-\delta_i)\underline{\nu_1} + (1 + \delta_i) \tag{52}$$

and

$$\underline{V_i} = [\delta_i/(1 + \delta_i)]\underline{\nu_1} + 1/(1 + \delta_i) \tag{53}$$

In these three equations the underscored voltages indicate normalized values; the voltages of the first two equations have been normalized to V_i while those of the last equation have been normalized to V_1. Typical curves for equations (51), (52) and (53) are shown in Figs. 17, 18 and 19, respectively. Note that the ranges of the variables in the figures are restricted to represent only the practical cases where the energy stored in capacitor C_1 is increased by the charging current ($V_1 > \nu_1$), and the loss factor is restricted to the realizable values ($0 < \delta_i < 1$). These curves present an easy graphical means of determining any one of the following parameters when the other two are known: input voltage V_i, output voltages ν_1 and V_1, and input loss factor δ_i. Once all the above parameters are determined, it becomes a simple matter to calculate losses, efficiency, etc.

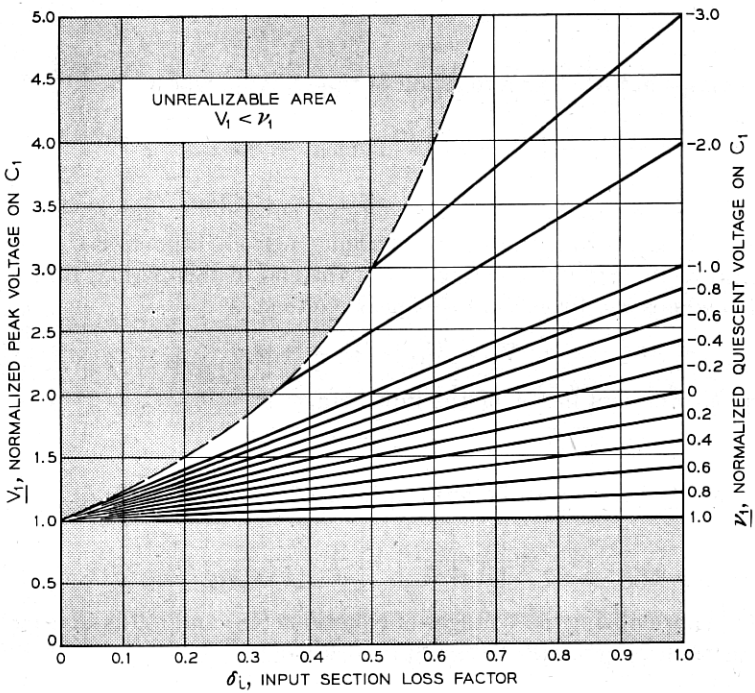

Fig. 17 — Straight line plot for the input section for V_i equals unity.

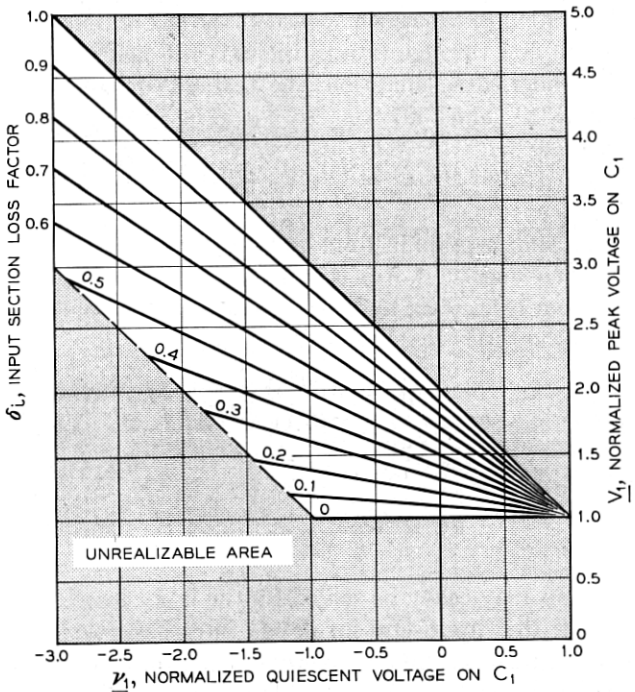

Fig. 18 — Straight line plot for the input section for V_i equals unity.

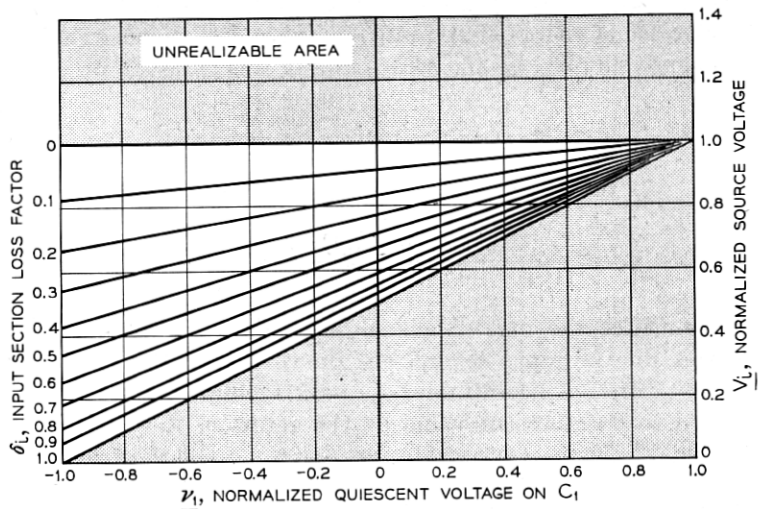

Fig. 19 — Straight line plot for the input section for V_1 equals unity.

Since the switch, S_i, has been opened at the end of the charging period, no current will flow through it until the switch is again triggered at time t_i equals T. Under these conditions the average current, $\bar{i}_i$, through the switch is from (41) and (50)

$$\bar{i}_i = \frac{C_1}{T}(V_1 - \nu_1) \tag{54}$$

Although a simple graphical method for determining the functions of energy has been suggested, it is still noteworthy to write these relations explicitly. From (41), (50), and (54), the energy per pulse, W_i, that is dissipated in the series resistance, R_i, is

$$W_i = \frac{\bar{i}_i^2 T^2(1 - \delta_i)}{2C_1(1 + \delta_i)} \tag{55}$$

or

$$W_i = \frac{C_1(1 - \delta_i)(V_1 - \nu_1)^2}{2(1 + \delta_i)} \tag{56}$$

These equations may easily be solved for the input loss factor, δ_1, yielding expressions that are useful for design purposes.

Since explicit relations for the energy loss per pulse have been derived, an expression for the efficiency, η_i, of the energy transfer from the source, V_i, to the first capacitor, C_1, may be written. From equations (55) and (56), respectively, two expressions for this efficiency, which is the ratio of the increase of energy stored in C_1 at the end of the charging period to the energy supplied by the source during this period, are

$$\eta_i = \frac{2C_1(1 + \delta_i)V_i - T(1 - \delta_i)\bar{i}_i}{2C_1(1 + \delta_i)V_i} \tag{57}$$

or

$$\eta_i = \frac{(1 + \delta_i)(V_1 + \nu_1)}{(1 + \delta_i)(V_1 + \nu_1) + (1 - \delta_i)(V_1 - \nu_1)} \tag{58}$$

To summarize the preceding analysis, typical voltage and current waveforms for the input section are shown in Fig. 20. Observe that capacitor C_1 after it has attained its peak voltage is not immediately discharged to its quiescent value by the action of the transfer chain. Instead this discharge is delayed by a period G_1, called the guard interval of the first transfer section. It was noted that the active switch at the end of the charging period, τ_i, was opened by a combination of circuit actions. Now some devices, such as a thyratron, require a definite time

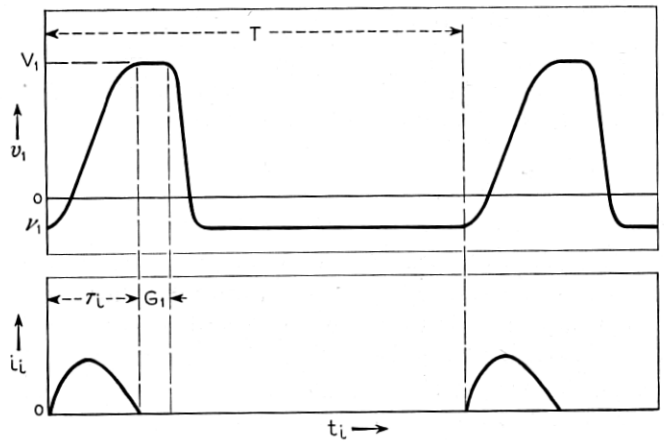

Fig. 20 — Typical waveforms for the input section.

period for deactivation to insure that the switch remains open. The guard interval, G_1, provides this period by forestalling the discharge action.

An expression that completely defines the operation of the input charging section would greatly facilitate the following endeavor to synthesize the over-all modulator performance. Such an expression is easily constructed by writing equations (50) and (54) in the following matrix form:

$$\begin{bmatrix} V_i \\ \overline{i_i} \end{bmatrix} = \begin{bmatrix} 1/(1+\delta_i) & \delta_i/(1+\delta_i) \\ C_1/T & -C_1/T \end{bmatrix} \begin{bmatrix} V_1 \\ \nu_1 \end{bmatrix} \tag{59}$$

Equation (59) relates the input and output conditions of the charging section in terms of the circuit constants independent of the time variable, t_i. Note that there is a similarity between this equation and the equation that relates the input and output voltages and currents of a four-terminal linear passive network by its $ABCD$ constants. The similarity is only in form; hence, the lower case letters *abcd* will be used to denote the constants of the above equation in the following fashion:

$$\begin{bmatrix} V_i \\ \overline{i_i} \end{bmatrix} = \begin{bmatrix} a_i & b_i \\ c_i & d_i \end{bmatrix} \begin{bmatrix} V_1 \\ \nu_1 \end{bmatrix} \tag{60}$$

where

$$a_i = 1/(1+\delta_i) \tag{61}$$

$$b_i = \delta_i/(1+\delta_i) \tag{62}$$

$$c_i = C_1/T \tag{63}$$

and

$$d_i = -C_1/T \tag{64}$$

These relations, as mentioned above, will be employed later.

TYPICAL TRANSFER SECTION

The j*th* or typical section of the transfer chain of Fig. 15, is shown in detail in Figure 21. According to the assumptions concerning switch operation, switch S_j will remain open as shown until the total available pulsed energy previously initiated by the charging section is stored in capacitor C_j. Consequently, at the time switch S_j closes, starting at time t_j equals zero, the current through the saturated j*th* thyractor is zero, and capacitor C_j is charged to its peak voltage V_j while C_k is still at its quiescent value ν_k. For these conditions, the current, i_j, through the

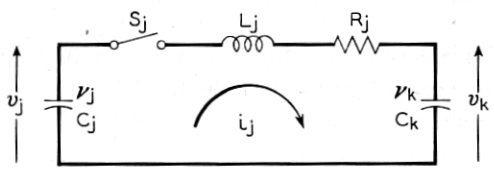

Fig. 21 — Equivalent circuit of a typical transfer section.

switch is of the form

$$i_j = \frac{V_j - \nu_k}{L_j\omega_j}\,\epsilon^{-\alpha_j t_j}\sin\omega_j t_j \tag{65}$$

where

$$V_j > \nu_k \tag{66}$$

$$\alpha_j = \frac{R_j}{2L_j} \tag{67}$$

$$\omega_j = \sqrt{\beta_j^2 - \alpha_j^2} \tag{68}$$

$$\beta_j = \sqrt{\frac{1+\lambda_j}{L_jC_j}} \tag{69}$$

and

$$\lambda_j = \frac{C_j}{C_k} \tag{70}$$

for the oscillatory case. This again is the only case of interest since the transfer current will eventually tend to reverse, driving the thyractor out of saturation and hence extinguishing the current. Under these conditions, it is seen from (65) that the period of current flow is τ_j, called the transfer period of the j*th* section, where

$$\tau_j = \frac{\pi}{\omega_j}. \tag{71}$$

The voltages across C_j and C_k as functions of time, t_j, v_j and v_k respectively, may be shown to be

$$v_j = V_j - \frac{V_j - \nu_k}{1 + \lambda_j}\left[1 - \left(\frac{\alpha_j}{\omega_j}\sin \omega_j t_j + \cos \omega_j t_j\right)\epsilon^{-\alpha_j t_j}\right] \tag{72}$$

and

$$v_k = \nu_k + \frac{\lambda_j(V_j - \nu_k)}{1 + \lambda_j}\left[1 - \left(\frac{\alpha_j}{\omega_j}\sin \omega_j t_j + \cos \omega_j t_j\right)\epsilon^{-\alpha_j t_j}\right] \tag{73}$$

Since as noted above the current has been unidirectional during the entire transfer period, the capacitor C_j will be charged to its minimum or quiescent voltage ν_j and capacitor C_k will be charged to its maximum voltage V_k at the end of this period. Hence, at time t_j equals τ_j (72) and (73) become

$$\nu_j = \left[1 - \frac{1 + \delta_j}{1 + \lambda_j}\right] V_j + \left[\frac{1 + \delta_j}{1 + \lambda_j}\right] \nu_k \tag{74}$$

and

$$V_k = \left[\lambda_j \frac{1 + \delta_j}{1 + \lambda_j}\right] V_j + \left[1 - \lambda_j \frac{1 + \delta_j}{1 + \lambda_j}\right] \nu_k \tag{75}$$

where, δ_j, the loss factor of the j*th* transfer section, is

$$\delta_j = \epsilon^{-\alpha_j \tau_j} \tag{76}$$

Rearrangement of equations (74) and (75) and normalization of the voltages to V_j (underscored voltages again represent normalized values) yield equations (77) and (78):

$$\underline{V_k} = \left[\frac{\delta_j}{1 + \delta_j}(1 - \underline{\nu_j})\right] \lambda_j + \left[\frac{\delta_j}{1 + \delta_j}\left(1 + \frac{\underline{\nu_j}}{\delta_j}\right)\right] \tag{77}$$

$$\underline{\nu_k} = \left[\frac{1}{1 + \delta_j}(\underline{\nu_j} - 1)\right] \lambda_j + \left[\frac{\delta_j}{1 + \delta_j}\left(1 + \frac{\underline{\nu_j}}{\delta_j}\right)\right] \tag{78}$$

which are both families of straight line functions of the variables λ_j and

$\underline{V_k}$ or $\underline{\nu_k}$, respectively. These families result when a particular value of loss factor, δ_j (any value between 0 and 1), is assigned and $\underline{\nu_j}$ is given a set of values within its permissible range (its maximum range is from -1 to 1; however, it is further restricted as will be demonstrated below).

Observe that both families of straight lines of equations (77) and (78) have the same zero intercept ($\lambda_j = 0$), namely

$$\underline{V_k}(\lambda_j = 0) = \underline{\nu_k}(\lambda_j = 0) = \frac{\delta_j}{1 + \delta_j}\left(1 + \frac{\underline{\nu_j}}{\delta_j}\right) \tag{79}$$

Also, it may be shown that for any value of $\underline{\nu_j}$ the family of lines of equation (77) will go through the point

$$(\lambda_j, \underline{V_k}) = \left(\frac{1}{\delta_j}, 1\right) \tag{80}$$

And similarly for any value of both $\underline{\nu_j}$ and δ_j the family of lines of equations (78) will go through the point

$$(\lambda_j, \underline{\nu_k}) = (-1, 1) \tag{81}$$

Hence, equations (77) and (78) present an easily constructed graphical method of displaying all possible quiescent and peak voltages on the two capacitors, C_j and C_k, for a particular value of δ_j and any value of capacitance ratio λ_j. Two such plots are shown in Figs. 22 and 23, one for the lossless case, δ_j equals unity, and the other for a practical case, δ_j equals $\frac{2}{3}$, respectively. With the latter type plot that accounts for circuit dissipation, the loss and efficiency involved in the transfer can quickly be computed since the energy storage in the capacitors before and after the transfer action are readily determined. Both these figures suggest that peak voltage amplification can be realized if λ_j is made greater than $1/\delta_j$. This interesting possibility will be discussed later.

In Figure 23, the shaded area is unrealizable and is defined by the following considerations. At the start of the transfer action energy is stored in capacitor C_j and C_k. Although, depending on the capacitance ratio, the energy storage in C_k may be greater, $\underline{\nu_k}$ must always be less than unity as seen from (66). Now, at the end of the transfer period the only condition of interest is the case where the energy storage, despite circuit dissipation, has been increased in C_k. This means that $\underline{V_k}$ must always be greater than $|\underline{\nu_k}|$. A line that includes all the points for V_k equal to $|\underline{\nu_k}|$ can readily be constructed graphically. Such a line is shown in Fig. 23, and all points below it represent conditions where $\underline{V_k}$ is less than $|\underline{\nu_k}|$, and consequently are unrealizable.

A figure that represents the general case with circuit dissipation is

shown in Figure 24. The four regions which are indicated in this figure are defined by the voltage conditions of Table I. A typical voltage waveform for each region is shown in Fig. 25. In this figure, capacitor C_j charges to its peak voltage over a time interval τ_h, the transfer period of the h*th* section which precedes the j*th* section in the transfer chain. Capacitor C_k is discharged in a time interval τ_k, the transfer period of the following or k*th* section. Again it should be noted that both capacitors C_j and C_k are not immediately discharged once they attain their peak

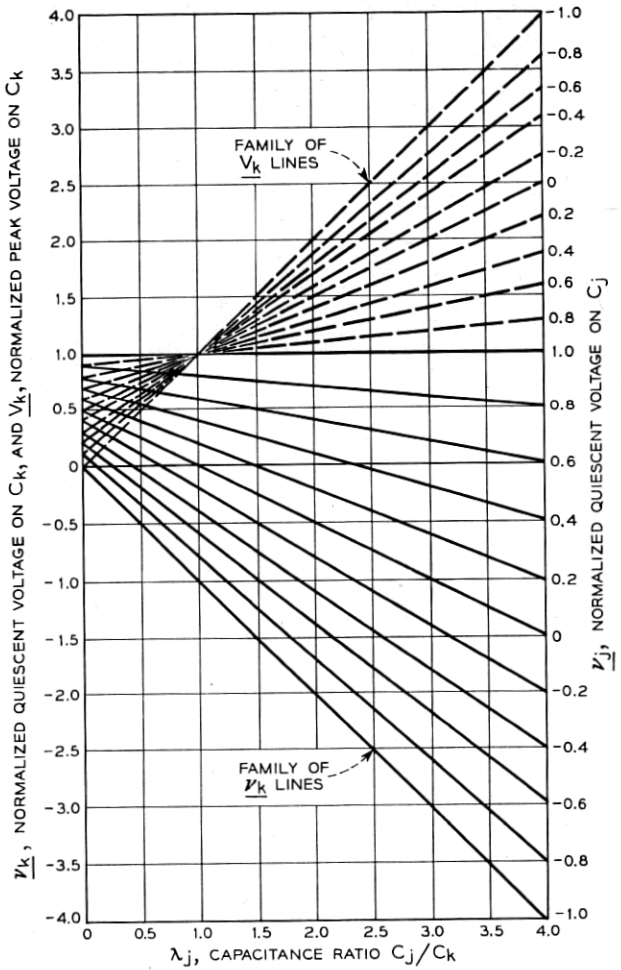

Fig. 22 — Straight line plot for a lossless transfer section, δ_j equals 1.

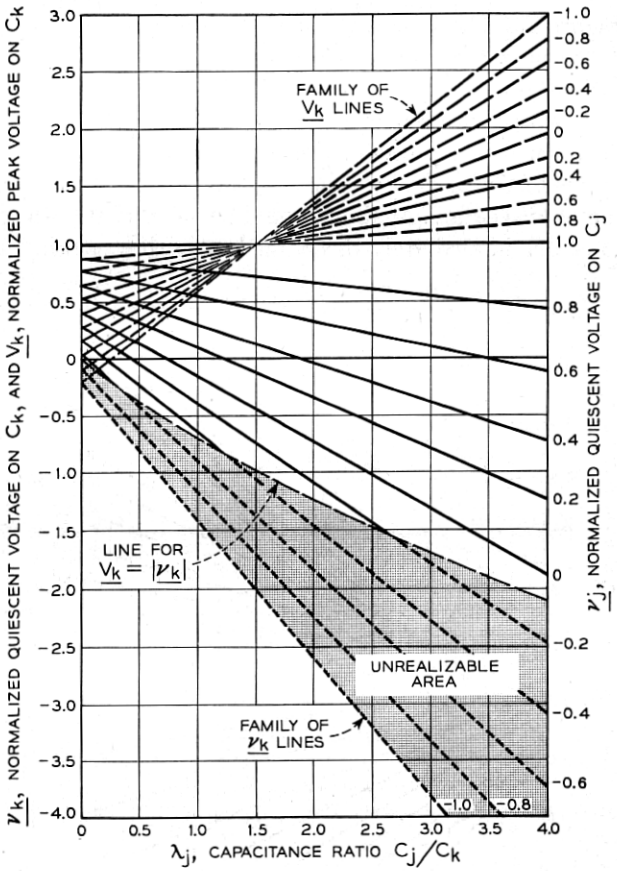

Fig. 23 — Straight line plot for a practical transfer section, δ_j equals $\frac{2}{3}$.

voltages but remain charged for a period of G_j and G_k, the guard intervals of the j*th* and k*th* transfer sections, respectively. This time delay, or guard interval, plays an important part both in permitting circuit operation without the necessity of bias windings on the thyractors and in designing these elements to operate properly even when wide production tolerances are allowed. This former aspect will be treated later. Capacitor C_1 that was discussed in the charging stage and C_k are discharged in the same manner as capacitor C_j.

Since the switch, S_j, has been opened at the end of the transfer period, no current will flow through it until the switch is again closed at time t_j equals T. Under these conditions the average current, $\bar{i}_j$, through the

TABLE I

Region	ν_j	ν_k
I	>0	>0
II	>0	<0
III	<0	>0
IV	<0	<0

switch from (65), (74) and (75) is

$$\bar{i}_j = \frac{C_j}{T}(V_j - \nu_j) \tag{82}$$

or

$$\bar{i}_j = \frac{C_k}{T}(V_k - \nu_k) \tag{83}$$

Although again a simple graphical method for determining the functions of energy has been suggested, explicit forms of these relations will be written. From equations (65), (74) and (75), the energy per pulse

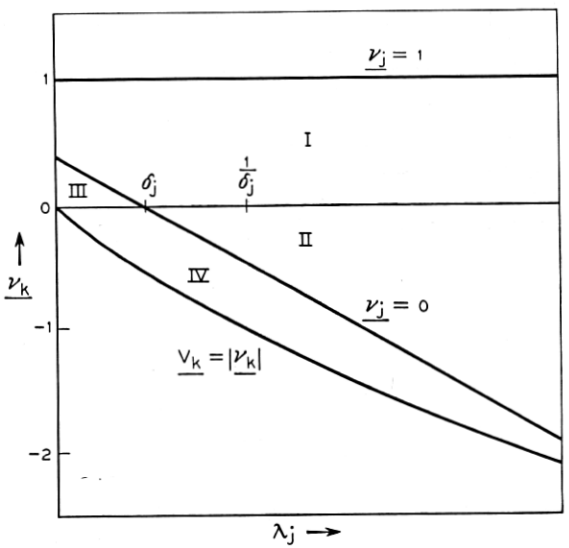

Fig. 24 — General straight line plot for a typical transfer section with losses, indicating the four regions of operation.

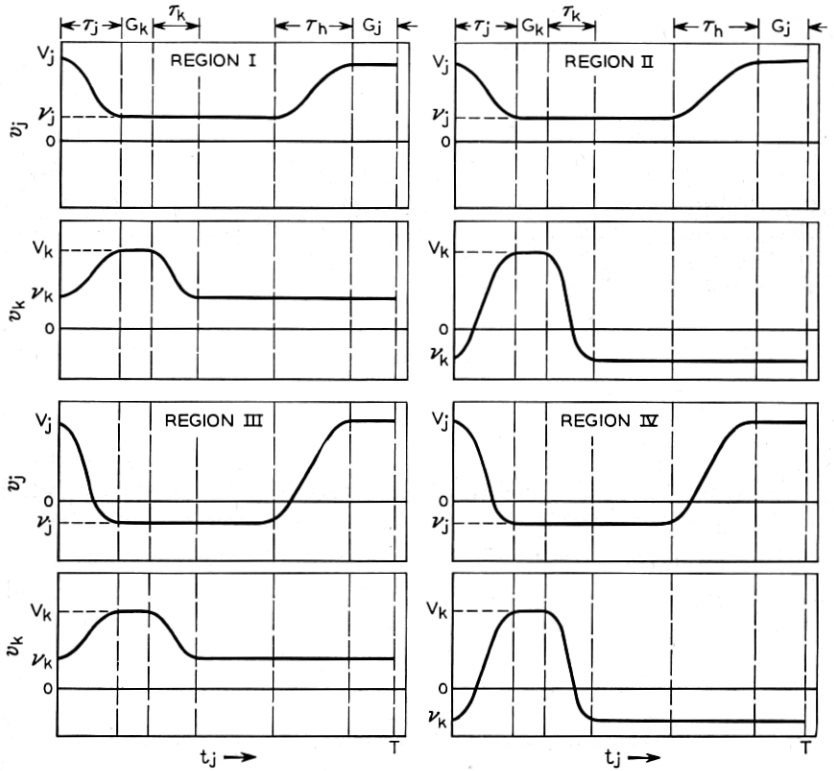

Fig. 25 — Typical voltage waveforms of a transfer section experienced in the four possible operating regions.

W_j, that is dissipated in the series resistance, R_j, is

$$W_j = \frac{C_j(V_j - \nu_j)^2(1 + \lambda_j)(1 - \delta_j)}{2(1 + \delta_j)} \tag{84}$$

or

$$W_j = \frac{C_k(V_k - \nu_k)^2(1 + \lambda_k)(1 - \delta_j)}{2\lambda_j(1 + \delta_j)} \tag{85}$$

These equations may be solved for the transfer loss factor, δ_j, which once again yield expressions that are useful in design computations.

From equations (84) and (85), expressions for the efficiency, η_j, of the energy transfer from capacitor C_j to C_k may be written. The resulting expressions for this efficiency, which is the ratio of the increase of energy

in C_k to the decrease of energy in C_j due to the transfer action, are

$$\eta_j = \frac{(1 + \delta_j)(V_j + \nu_j) - (1 + \lambda_j)(1 - \delta_j)(V_j - \nu_j)}{(1 + \delta_j)(V_j + \nu_j)} \tag{86}$$

and

$$\eta_j = \frac{\lambda_j(1 + \delta_j)(V_k + \nu_k)}{\lambda_j(1 + \delta_j)(V_k + \nu_k) + (1 + \lambda_j)(1 - \delta_j)(V_k - \nu_k)} \tag{87}$$

Up to this point, little has been said about how the thyractors of the transfer chain switch in the manner as outlined in the assumptions. Such operation is now worth consideration. In order to realize the equivalent circuit of Fig. 21, the j*th* thyractor must have the hysteresis loop shown in Figure 26. It was assumed that S_j closes at time t_j equals zero when capacitor C_j is charged to its maximum voltage, V_j. The switch closure is associated with the saturation of the j*th* thyractor. Assume the core at this time is at the positive saturation point designated by $+B_s$ in Fig. 26. During the current discharge it moves out to some value of maximum field intensity represented by point e. For any practical core material this value of H, which can be derived from (65), is normally hundreds of times its coercive force. At time equal to τ_j the current is again zero, and hence the core has returned to $+B_s$. It was noted before, in the discussion following (65), that the transfer current by its tendency to reverse drives the core into an unsaturated region. This region, lying between $+B_s$ and $-B_s$, has extremely high permeability; consequently, the high thyractor impedance cuts off the current. In order

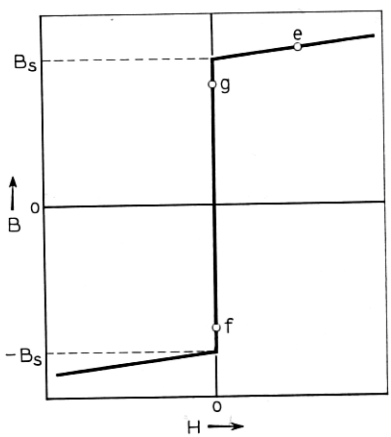

Fig. 26 — Hysteresis loop of the j*th* thyractor.

to best utilize the core material, the core must be driven to some point near or equal to $-B_S$ such as f before the next pulse that is initiated by the charging stage starts to recharge C_j to its peak voltage.

Rather than use a bias winding to establish a polarizing field as suggested by Melville, the resetting action can be accomplished by insuring that the proper voltage waveform exists across the thyractor. The flux density swing in the core is proportional to the time integral of voltage across the main winding. This voltage for the j*th* thyractor inductor, which is merely the difference of the voltages on capacitors C_j and C_k, over the pulse repetition period T can have any of the three forms shown in Fig. 27 depending on the quiescent values, ν_j and ν_k. To avoid confusion, the voltage across this element during the period τ_j is not shown, since it was demonstrated that the core over this period will experience no net flux swing due to such voltages. As can be verified from Figs. 22 and 23, these waveforms are associated with the values λ_j, indicated in the figure.

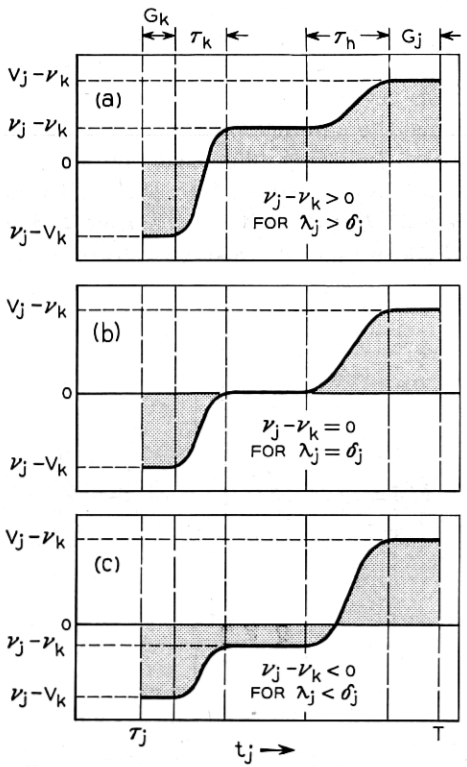

Fig. 27 — Possible voltage waveforms across the j*th* thyractor.

If the net area under the voltage curve from time t_j equals τ_j to T is zero, the core magnetization will have traversed a path similar to $B_s g f g B_s$ of Fig. 26. The subsequent saturation of the core and resulting transfer action will complete the cycle in the manner previously described by driving the magnetization from $+B_s$ to e and returning to $+B_s$. The negative area in Fig. 27 swings the core on the first part of this path from $+B_s$ to its smallest value of flux density represented by point f. This value of flux density must be greater than $-B_s$ in order to avoid secondary saturations. Furthermore, for the most economical utilization of the core material, the core magnetization should reach this value approximately at the start of the charging period of capacitor C_j as in Figure 27(b) or (c). The flux swing resulting from the positive area up to the time capacitor C_j is charged to its peak voltage should bring the core to some point less than $+B_s$ such as g on the loop. Capacitor C_j will then remain charged for a length of time G_j, the guard interval, such that the additional area causes the core to saturate completing the path in the unsaturated region.

Now it can be demonstrated from (74) and (75) that the peak positive voltage across the thyractor is always greater than the magnitude of the peak negative voltage for any practical transfer section ($\delta_j < 1$). Since pulse shortening is required in successive transfer sections, that is, the transfer periods of successive sections must be smaller and smaller, it is obvious from Fig. 27(b), that for λ_j equals δ_j, the only manner in which to make the net area under the voltage curve exactly zero, as is required, is to make the guard interval of the following section, G_k, greater than the guard interval of the j*th* section, G_j.

From this line of reasoning, it is seen from Figure 27(a) that for λ_j greater than δ_j the guard interval G_k must be made even larger. However, for λ_j less than δ_j as in Fig. 27(c), guard interval shortening in addition to pulse shortening may be realized. The advantages of such operation will be discussed in the composite analysis of the input section and transfer chain that follows.

To complete the analysis of the typical transfer section, it is possible to write an expression, similar to the one derived for the input section, that relates the peak and quiescent voltages on the capacitors C_j and C_k. Rearrangement of equations (74) and (75) admits of the following:

$$\begin{bmatrix} V_j \\ \\ \nu_j \end{bmatrix} = \left[\begin{array}{c|c} \dfrac{1+\lambda_j}{\lambda_j(1+\delta_j)} & 1 - \dfrac{1+\lambda_j}{\lambda_j(1+\delta_j)} \\ \hline \dfrac{1+\lambda_j}{\lambda_j(1+\delta_j)} - \dfrac{1}{\lambda_j} & 1 + \dfrac{1}{\lambda_j} - \dfrac{1+\lambda_j}{\lambda_j(1+\delta_j)} \end{array}\right] \begin{bmatrix} V_k \\ \\ \nu_k \end{bmatrix} \tag{88}$$

or

$$\begin{bmatrix} V_j \\ v_j \end{bmatrix} = \begin{bmatrix} a_j & b_j \\ c_j & d_j \end{bmatrix} \begin{bmatrix} V_k \\ v_k \end{bmatrix} \tag{89}$$

where

$$a_j = \frac{1 + \lambda_j}{\lambda_j(1 + \delta_j)} \tag{90}$$

$$b_j = 1 - \frac{1 + \lambda_j}{\lambda_j(1 + \delta_j)} \tag{91}$$

$$c_j = \frac{1 + \lambda_j}{\lambda_j(1 + \delta_j)} - \frac{1}{\lambda_j} \tag{92}$$

and

$$d_j = 1 + \frac{1}{\lambda_j} - \frac{1 + \lambda_j}{\lambda_j(1 + \delta_j)} \tag{93}$$

More will be said later concerning the application of these equations in the evaluation of the modulator performance.

DAMPING SECTION

Since the magnetron current at the end of the RF pulse is extinguished when considerable energy is still stored in circuit inductances and capacitances, the magnetron voltage pulse decays in an oscillatory fashion.[8] Normally, this oscillation will be reinforced by energy remaining in the energy storage device of the modulator. The resultant negative voltage peaks generally give rise to low-power secondary RF pulses which are most undesirable since they occur during the listening period of the radar, masking even the strongest echos.

The undesirable voltage transient may be avoided by minimizing the inductively stored energy and by dissipating the capacitively stored energy with the damping section shown in Fig. 14. In this section the thyractor, called a damping thyractor, is designed to saturate at the end of the main RF pulse. The resistance in series with this element is chosen to effectively terminate the energy storage device, discharging it before oscillations can arise. The saturated inductance of the damping thyractor is proportioned such that the distributed capacitance across the magnetron is terminated in a slightly underdamped circuit in order to complete its discharge in a relatively short period. Hence, the magnitude of

[8] *Pulse Generators*, op. cit.

the positive voltage backswing across the magnetron is controlled by the degree of damping and can be reduced to such a value that no objectionable voltage reversal will follow.

The damping circuit that exists across the distributed capacitance when the damping thyractor saturates could be analyzed in the same fashion as the two preceding type sections. However, since this occurs after the generation of the RF pulse, it would contribute little to the synthesis of the over-all performance of the modulator and hence only the results will be briefly noted.

When the damping thyractor saturates, the distributed capacitance across the magnetron is charged to the magnetron firing voltage, $-V_M$. For an underdamped circuit, the current through the thyractor, similar to that of (41), discharges this capacitance over a period τ_d, the damping period. At the end of this period, the current is extinguished by its tendency to reverse through the thyractor, and the magnetron capacitance remains charged to some positive potential, v_d, where

$$v_d = \delta_d V_M \tag{94}$$

The loss factor, δ_d, which is also the backswing ratio in this case, is defined in terms of the circuit parameters of the damping section similar to the form evolved for the input loss factor, δ_i, of (49). It may be demonstrated that the shortest damping period, $\pi R_T C_d$ seconds, is realized when the total series inductance of the damping path is made equal to $R_T^2 C_d/2$ henries, where R_T is the total resistance referred to the same winding as the distributed capacitance, C_d. The backswing ratio for this condition is $\epsilon^{-\pi}$, about four per cent. Hence, the damping circuit is completely defined by the above relations since R_T is made to be the characteristic impedance of the energy storage device and C_d is fixed by the pulse transformer and magnetron combination.

Finally the damping efficiency, η_d, that is the ratio of the energy dissipated over the damping period to the energy originally stored in C_d is:

$$\eta_d = 1 - \delta_d^2 \tag{95}$$

For the condition of minimum damping time, the efficiency is 99.8 per cent. This figure was derived on the basis that no energy was left in the *PFN* at the beginning of the damping period.

COMPOSITE ANALYSIS OF THE INPUT SECTION AND TRANSFER CHAIN

In Part I it was explained that in order to obtain pulse shortening successive thyractors in the transfer chain must have descending values of saturating flux linkages. Part of these flux linkages in any thyractor

are required for the charging of the input capacitor of the particular transfer section associated with the thyractor. The remainder provide the thyractor guard interval. In the first section the amount of flux linkages required for the guard interval may be quite small compared to those needed for the input charging time. However, if the successive capacitance ratios are such that increasing guard intervals must be employed in order to operate without bias, the proportion of flux linkages needed for successive guard intervals becomes larger and larger. Eventually, it will become necessary to increase the saturating flux linkages of successive thyractors, and hence not pulse shortening but pulse lengthening will result.

$$\overline{i_h} = \frac{C_h}{T}(V_h - \nu_h),$$

$$\overline{i_h} = \frac{C_j}{T}(V_j - \nu_j) = \overline{i_j} = \frac{C_j}{T}(V_j - \nu_j),$$

$$\overline{i_j} = \frac{C_k}{T}(V_k - \nu_k) = \overline{i_k} = \frac{C_k}{T}(V_k - \nu_k),$$

$$\overline{i_k} = \frac{C_l}{T}(V_l - \nu_l)$$

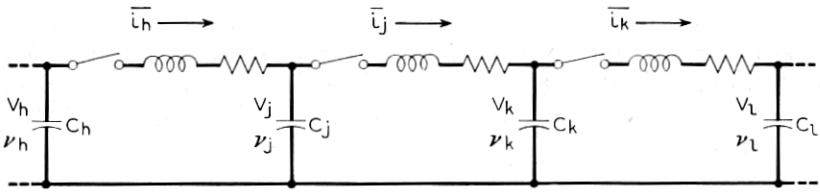

Fig. 28 — Illustration of current continuity by extension of the average current relations of equations (82) and (83).

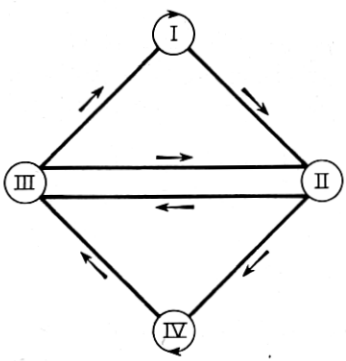

Fig. 29 — Representation of the possible operating regions of successive transfer sections of the transfer chain.

These conditions occur when the sections have capacitance ratios that are greater than their loss factors. The only advantage in such operation would be to obtain the peak voltage amplification which results when this ratio is increased to a value greater than the reciprocal of the loss factor. This further increase results in restricting the pulse shortening to a smaller number of sections if bias free operation is still to be maintained. On the other hand, if the capacitance ratios are smaller than the loss factors, there is no theoretical limit on the number of sections in which pulse shortening can be realized since guard interval shortening is possible. However, the required voltage amplification would then have to be provided by a pulse transformer.

From the average current relations of (51), (82) and (83), it is observed that current continuity through the successive sections does not depend upon the values of δ and λ. Fig. 28 illustrates this point. However, since the peak and quiescent voltages out of a section must equal the peak and quiescent voltages into the next section, there are restrictions on the regions in which two adjacent sections may operate. These restrictions can be seen by inspecting either Table I or Fig. 25. Fig. 29 indicates all the possible transfer chains in the following manner: any number of successive sections up to an entire chain that all operate in either region I or IV are possible. This is indicated by the arrowhead on the circle inscribing the Roman numerals I and IV in the figure. Beyond these possibilities, successive sections must be operating in the regions indicated by the arrows. For example, a section operating in region II must be followed by one that operates either in region III or IV.

When these voltage restrictions are applied to a modulator consisting of an input section and a transfer chain of n sections, the following relations result:

$$\begin{bmatrix} V_i \\ \bar{i}_i \end{bmatrix} = \begin{bmatrix} a_i & b_i \\ c_i & d_i \end{bmatrix} \begin{bmatrix} V_1 \\ \nu_1 \end{bmatrix} \tag{96}$$

$$\begin{bmatrix} V_1 \\ \nu_1 \end{bmatrix} = \begin{bmatrix} a_1 & b_1 \\ c_1 & d_1 \end{bmatrix} \begin{bmatrix} V_2 \\ \nu_2 \end{bmatrix} \tag{97}$$

. . . . . .

$$\begin{bmatrix} V_j \\ \nu_j \end{bmatrix} = \begin{bmatrix} a_j & b_j \\ c_j & d_j \end{bmatrix} \begin{bmatrix} V_k \\ \nu_k \end{bmatrix} \tag{98}$$

. . . . . .

$$\begin{bmatrix} V_n \\ \nu_n \end{bmatrix} = \begin{bmatrix} {}_n & b_n \\ c_n & d_n \end{bmatrix} \begin{bmatrix} V_0 \\ \nu_0 \end{bmatrix} \tag{99}$$

from which follows:

$$\begin{bmatrix} V_1 \\ \nu_1 \end{bmatrix} = \begin{bmatrix} a_{1n} & b_{1n} \\ c_{1n} & d_{1n} \end{bmatrix} \begin{bmatrix} V_0 \\ \nu_0 \end{bmatrix} \tag{100}$$

and

$$\begin{bmatrix} V_i \\ -i_i \end{bmatrix} = \begin{bmatrix} a_{in} & b_{in} \\ c_{in} & d_{in} \end{bmatrix} \begin{bmatrix} V_0 \\ \nu_0 \end{bmatrix} \tag{101}$$

where

$$\begin{bmatrix} a_{1n} & b_{1n} \\ c_{1n} & d_{1n} \end{bmatrix} = \begin{bmatrix} a_1 & b_1 \\ c_1 & d_1 \end{bmatrix} \begin{bmatrix} a_2 & b_2 \\ c_2 & d_2 \end{bmatrix} \cdots \begin{bmatrix} a_j & b_j \\ c_j & d_j \end{bmatrix} \cdots \begin{bmatrix} a_n & b_n \\ c_n & d_n \end{bmatrix} \tag{102}$$

and

$$\begin{bmatrix} a_{in} & b_{in} \\ c_{in} & d_{in} \end{bmatrix} = \begin{bmatrix} a_i & b_i \\ c_i & d_i \end{bmatrix} \begin{bmatrix} a_{1n} & b_{1n} \\ c_{1n} & d_{1n} \end{bmatrix} \tag{103}$$

Equation (100), which relates the input and output voltages of the transfer chain, can also be used to determine the voltages on any capacitor if the conditions on any one capacitor are known. This is readily accomplished by letting n equal the number of sections that separate the two capacitors in question. The relation of (101) is of particular interest since the over-all operation is completely defined by the network parameters alone. If either the input or output conditions are given, the other is determined.

Equation (101) was derived on the basis that energy is stored in the capacitors during inactive periods and that the thyractors do not experience secondary saturations. Experimental evidence has verified that a modulator whose capacitors are initially discharged can build up to these stable conditions. But this cannot easily be predicted, hence empirical methods must be used to ascertain that reasonable guard intervals exist during this initial build-up period.

Obviously, the special case that was originally discussed by Melville and was treated in Part II in which all quiescent voltages are zero will operate stably. As can readily be seen from Fig. 24, this requires that the capacitance ratio of each section be equal to the section loss factor. However, since such conditions do not facilitate pulse shortening when bias-free operation is desired, smaller capacitance ratios with the resulting quiescent voltages should be employed.

Since a number of transformers with any reasonable turns ratio can

be used, the voltage level in any portion of the modulator is not rigidly fixed by the input and output requirements. In choosing these levels, paramount consideration should be given to the operational requirements imposed upon the active switching device, such as the peak inverse voltage, peak current, duty cycle, etc., so that long life may be realized. Since the size of the capacitors is primarily determined by the energy per pulse and the size of the thyractors by this, the over-all pulse shortening and the number of transfer sections, the voltage level affects these elements very little unless it is increased to a point where the end margins must be larger than those required for purely mechanical reasons. This may become important when the required output pulse is greater than 10,000 volts. It should be noted that although a larger number of sections may radically reduce the total amount of core material, and hence the losses, the size of the modulator will increase considerably since additional capacitors are required. These factors make any general theoretical attempt to ascertain the optimum design of little value. Present design experience on high-power modulators has indicated that usually no more than three or four transfer sections are required.

COMPOSITE ANALYSIS OF THE HOMOGENEOUS GEOMETRIC CASE

A homogeneous geometric modulator, that is a modulator composed of sections that have identical loss factors and capacitance ratios, can be analyzed with much less difficulty than a completely general modulator wherein each section is different and distinct. Such an analysis may be useful as a first approximation to the response of any geometric modulator provided that the loss factor of the homogeneous modulator is judiciously chosen. Furthermore, it will indicate the best performance attainable when the loss factor is made unity, and the methods outlined will serve as a guide for analyzing any modulator.

Consider a homogeneous geometric modulator composed of an input section and n transfer sections. For such a modulator[9]

$$\delta_i = \delta_1 = \delta_2 = \cdots \delta_n = \delta \tag{104}$$

and

$$\lambda_1 = \lambda_2 = \cdots \lambda_n = \lambda \tag{105}$$

Since all transfer sections will now have the same network constants,

[9] The value of any capacitor and the sum of all the capacitance in the chain can be explicitly written in terms of either the input or output capacitor by employing the well-known relations derived for a geometric progression.

abcd, (102) can be written in the following form:

$$\begin{bmatrix} a_{1n} & b_{1n} \\ c_{1n} & d_{1n} \end{bmatrix} = \begin{bmatrix} a & b \\ c & d \end{bmatrix}^n \tag{106}$$

From equations (90) through (93) inclusive, it may be demonstrated that for this particular modulator:

$$a_{1n} = \frac{(1+\lambda)(\lambda^n - 1)}{(1+\delta)(\lambda^{n+1} - \lambda^n)} - \frac{\lambda^{n-1} - 1}{\lambda^n - \lambda^{n-1}} \tag{107}$$

$$b_{1n} = \frac{\lambda^n - 1}{\lambda^n - \lambda^{n-1}} - \frac{(1+\lambda)(\lambda^n - 1)}{(1+\delta)(\lambda^{n+1} - \lambda^n)} \tag{108}$$

$$c_{1n} = \frac{(1+\lambda)(\lambda^n - 1)}{(1+\delta)(\lambda^{n+1} - \lambda^n)} - \frac{\lambda^n - 1}{\lambda^{n+1} - \lambda^n} \tag{109}$$

$$d_{1n} = \frac{\lambda^{n+1} - 1}{\lambda^{n+1} - \lambda^n} - \frac{(1+\lambda)(\lambda^n - 1)}{(1+\delta)(\lambda^{n+1} - \lambda^n)} \tag{110}$$

It is interesting to note that the determinant of the square matrix composed of the above elements equals $1/\lambda^n$. In addition note that if λ is made equal to δ, c_{1n} and d_{1n} become zero and unity respectively. This means from equation (100) that the quiescent voltages on all capacitors are identical and will all be made zero if capacitor C_0 is completely discharged by the output and damping sections. This substantiates what has previously been deduced in the general discussion of the composite input section and transfer chain arrangement.

The final matrix multiplication indicated in equation (103) can be performed with the aid of (61) through (64) yielding:

$$a_{in} = \frac{\delta}{1+\delta} + \frac{(1-\delta)(\lambda^{n+1} - 1)}{(1+\delta)(\lambda^{n+1} - \lambda^n)} \tag{111}$$

$$b_{in} = \frac{\delta}{1+\delta} - \frac{(1-\delta)(\lambda^n - 1)}{(1+\delta)(\lambda^{n+1} - \lambda^n)} \tag{112}$$

$$c_{in} = C_0/T \tag{113}$$

$$d_{in} = -C_0/T \tag{114}$$

The determinant of the square matrix composed of the above elements is $-C_0/T$.

From (101) and the preceding results the efficiency, η, of the energy

transfer from the dc source to the output capacitor is

$$\eta = \frac{\frac{1}{2}(1+\delta)(\lambda^{n+1}-\lambda^{n})\left[1+\frac{\nu_0}{V_0}\right]}{(\lambda^{n+1}-1)\left[1+\delta\frac{\nu_0}{V_0}\right]-(\lambda^{n}-1)\left[\delta+\frac{\nu_0}{V_0}\right]} \tag{115}$$

For the special case previously discussed in which all quiescent voltages were zero, that is, the case which results when ν_0 equals zero and λ equals δ, the efficiency becomes

$$\eta = \tfrac{1}{2}\delta^{n}(\delta+1) \tag{116}$$

Part IV — Conclusions

The analyses of the ac- and dc-charged modulators in the two preceding parts, although approximate to some degree, do provide a reasonable understanding of observed performance. This work has indicated the manner in which automatic core resetting in both devices can be achieved in all thyractors but the first of the ac-charged arrangement. All the regions of operation of a section of the transfer chain have been explored and have yielded the possibility of obtaining voltage amplification. However, such operation limits the pulse shortening that can be attained in the modulator; consequently, a transformer is still employed to provide the necessary voltage step-up.

Three practical innovations, in addition to the automatic core resetting, have been suggested. First, in order to provide short duration pulses without undue complication of the pulse transformer, the output thyractor section has been placed on the load side of this transformer. Second, a damping thyractor is employed such that the residual energy stored in the modulator after the generation of the main RF pulse can be safely dissipated without causing RF after pulsing. Both of these innovations can also be applied to other pulse modulators. And last, a dc-charged arrangement that provides still another means of automatic core resetting is presented in which the thyratron that may be required can be operated with its cathode at ground potential.

Several experimental ac- and dc-charged magnetic modulators that embody the automatic resetting feature without pulse amplification in the transfer chain have been developed. Fig. 30 illustrates an ac-charged modulator that provides an output pulse length of less than 0.1 microsecond. This very short pulse length has been achieved by placing the output thyractor, which has a ¼ mil molybdenum permalloy tape core, on the load side of the pulse transformer. The damping thyractor prin-

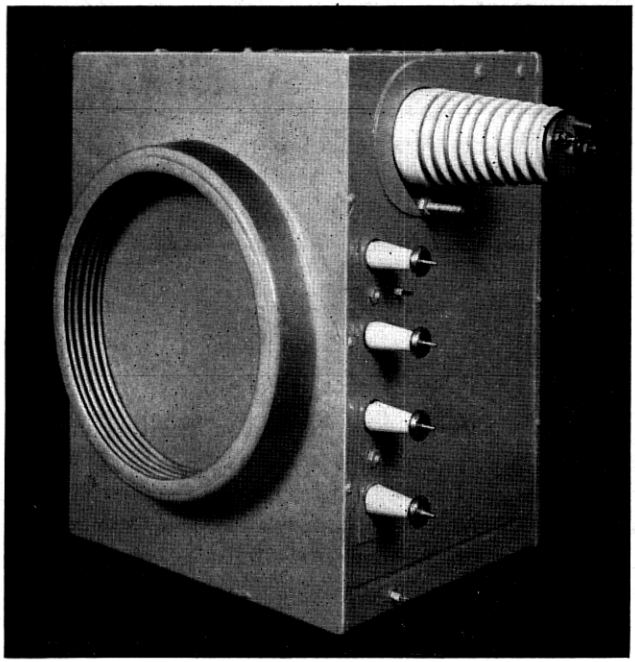

Fig. 30 — Experimental ac-charged magnetic modulator for a pulse duration of less than 0.1 microsecond.

ciple has been successfully employed in line type modulators as well as in these magnetic modulators. However, the grounded thyratron arrangement possible in the dc-charged case has not yet been incorporated in any design.

LIST OF SYMBOLS

	Quantity*
a	Section, chain or modulator constant
A	Area
b	Section, chain or modulator constant
B	Flux density
c	Section, chain or modulator constant
C	Capacitance
d	Section, chain or modulator constant
G	Guard interval
i	Instantaneous current

$\bar{i}$	Average current
I	Peak or constant current
L	Inductance
n	Number of sections in the transfer chain
N	Number of turns of wire
R	Resistance
t	Time
T	Pulse repetition period
v	Instantaneous voltage
V	Peak or constant voltage
$\underline{V}$	Normalized peak or constant voltage
W	Energy
X	Thyractor reference designation
α	Reciprocal of time constant
β	Constant, $\sqrt{\omega^2 + \alpha^2}$
δ	Loss factor
η	Efficiency
λ	Capacitance ratio
ν	Quiescent voltage
$\underline{\nu}$	Normalized quiescent voltage
τ	Time interval
ϕ	Magnetic flux
ω	Angular frequency

* All quantities are in rationalized MKS units.

CORRECTION

A. Uhlir, Jr., author of the paper *The Potentials of Infinite Systems of Sources and Numerical Problems in Semiconductor Engineering*, which appeared in the January, 1955, issue of the B.S.T.J., pages 105 to 128, has brought the following corrections to the attention of the editors.

In the last text sentence on page 107, for Q read P.

On page 124, equation (37) contains the term

$$-2 \ln \frac{\sinh \pi\lambda/k}{\pi\lambda/k}$$

This term should be

$$-2 \ln \frac{\sinh \pi\lambda/k}{2\pi/k}$$